XIX. NEUROLOGY*

L. Stark
S. Asano
F. H. Baker
G. Gottlieb
H. T. Hermann
J. C. Houk
R. Howland
G. P. Nelson
C. Northrup
Y. Okabe
M. Okajima
R. C. Payne
Julia H. Redhead
Helen E. Rhodes
P. R. Samson
V. Sanchez
A. Sandberg
G. Sever
J. Simpson
I. Sobel
S. F. Stanton
J. Stark
Y. Takahashi
E. Van Horn
P. A. Willis
L. R. Young
W. Zapol

A. DIGITAL-COMPUTER DIAGNOSIS OF THE ELECTROCARDIOGRAM BY USING PATTERN-RECOGNITION TECHNIQUES

The use of programmed digital computers as general pattern classification and recognition devices is one phase of the current lively interest in artificial intelligence. It is important to choose a class of signals which is, at present, undergoing a good deal of visual inspection by trained people for the purpose of pattern recognition. In this way comparisons between machine and human performance may be obtained. A practical result also serves as additional motivation. Clinical electrocardiograms make up such a class of signals.

The electrocardiogram, EKG, as abbreviated by Einthoven, is a repetitive signal,

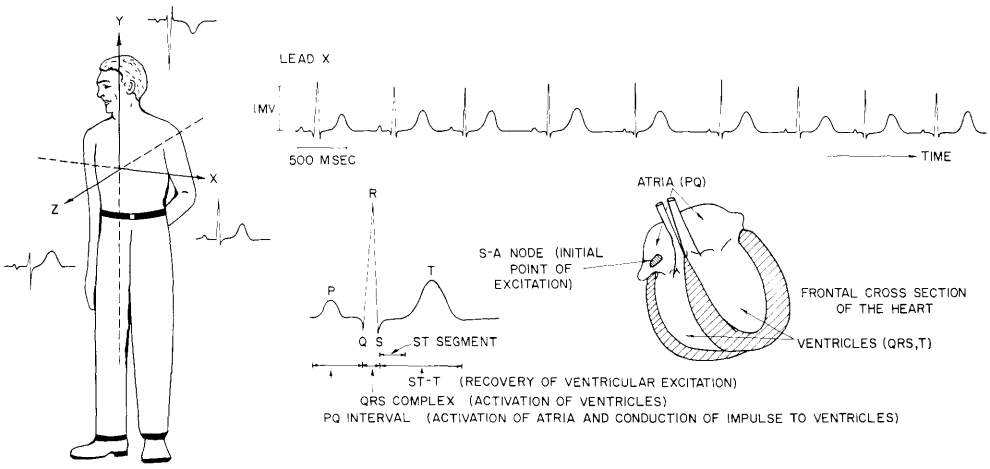

Fig. XIX-1. Electrocardiogram. Coordinate system for heart vector is illustrated at the left (Schmitt's SVEC III lead system) with X, Y, Z components for one heart-beat cycle. Time variation in beat-to-beat interval and in amplitude is seen in time function on the upper right-hand side. Some EKG terminology and heart anatomy are presented on the lower right-hand side.

*This research is supported in part by the U.S. Public Health Service (B-3055, B-3090), the Office of Naval Research (Nonr-609(39)), the Air Force (AF33(616)-7282, AF49(638)-1130), and the Army Chemical Corps (DA-18-108-405-Cml-942); and in part by the National Science Foundation (Grant G-16526).

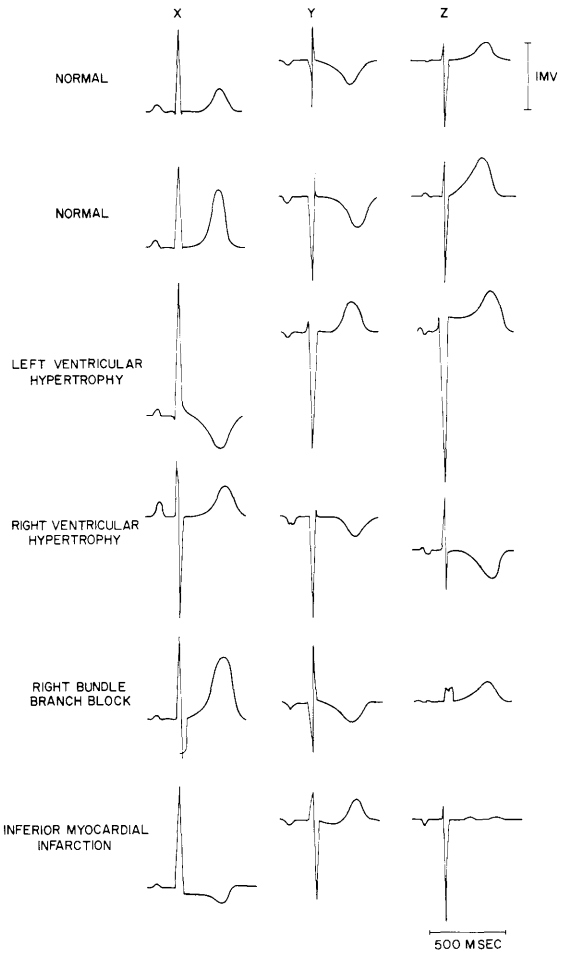

Fig. XIX-2. Normal and several abnormal EKG patterns in Schmitt's lead system. (Adapted from Nakagawa.[1])

not much contaminated by noise, but with some time variation as shown in Fig. XIX-1. It has three phases, PQ, QRS, and ST-T, associated with different stages in the electrical excitation of the heart. Cardiologists have empirically associated abnormal patterns,[1] examples of which are shown in Fig. XIX-2, with various pathological conditions, and their importance in clinical diagnosis is universally accepted. Human recognition of these EKG patterns continues to employ numerous, highly paid specialists.

Our approach to the problem centers upon the use of multiple adaptive matched filters that classify normalized signals. The present report will give some of the background for the application of this method.

Preliminary studies will be reported on later which will give specific details of various aspects of our program. We hope to test our methods by on-line processing of real data.

The EKG signal may be led off from the body by means of a matrix of resistors in order to obtain three relatively orthogonalized components as developed by Otto Schmitt of the University of Minnesota,[2,3] although most often less-sophisticated methods are used. Recently three groups have been studying automatic digital-computer processing.

Pipberger, Stallmann, and their collaborators[4-7] have been collecting clinical material from the Veterans Administration hospital system. Their data were first subjected to "point recognition" (which will be discussed below), and then numerous parameters, especially the "ventricular gradient," have been extracted. Woodbury and Cady[8,9] have summarized the EKG by means of several Fourier coefficients and have been able to distinguish the "left ventricular hypertrophy" pattern from the normal. Steinberg, Rikli, and their collaborators[10,11] have effectively used factor analysis and EKG parameter amplitude and duration for pattern recognition. A similar approach has been used

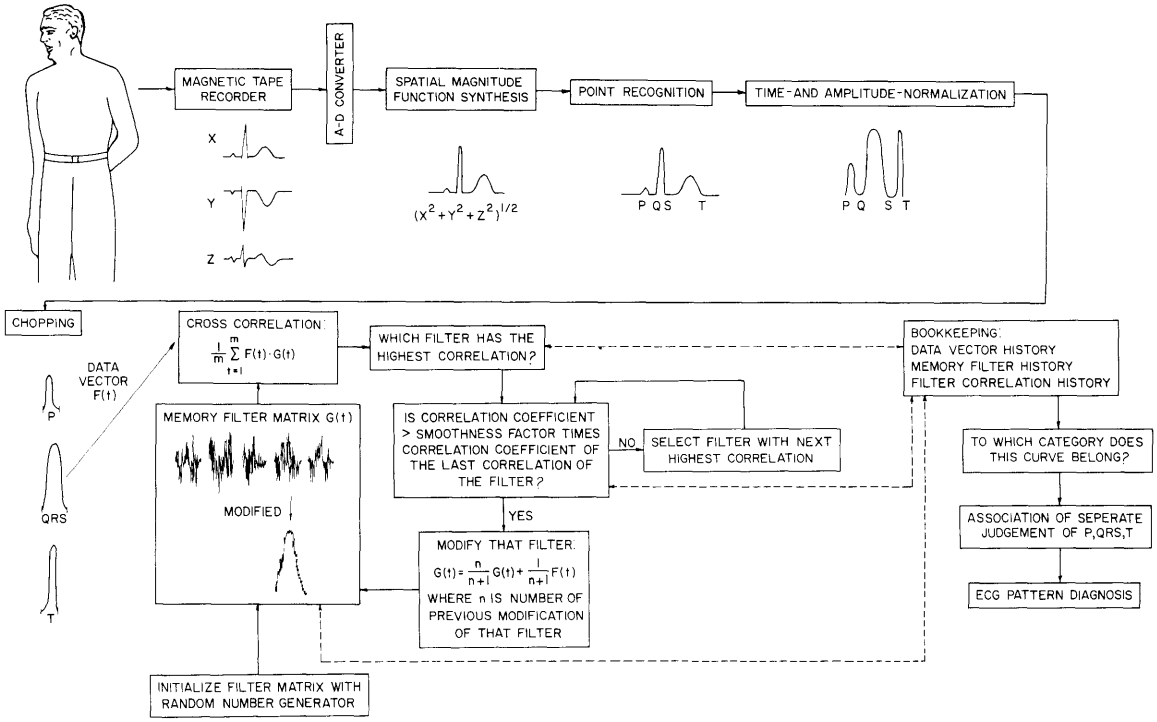

Fig. XIX-3. EKG data-processing system for pattern diagnosis.

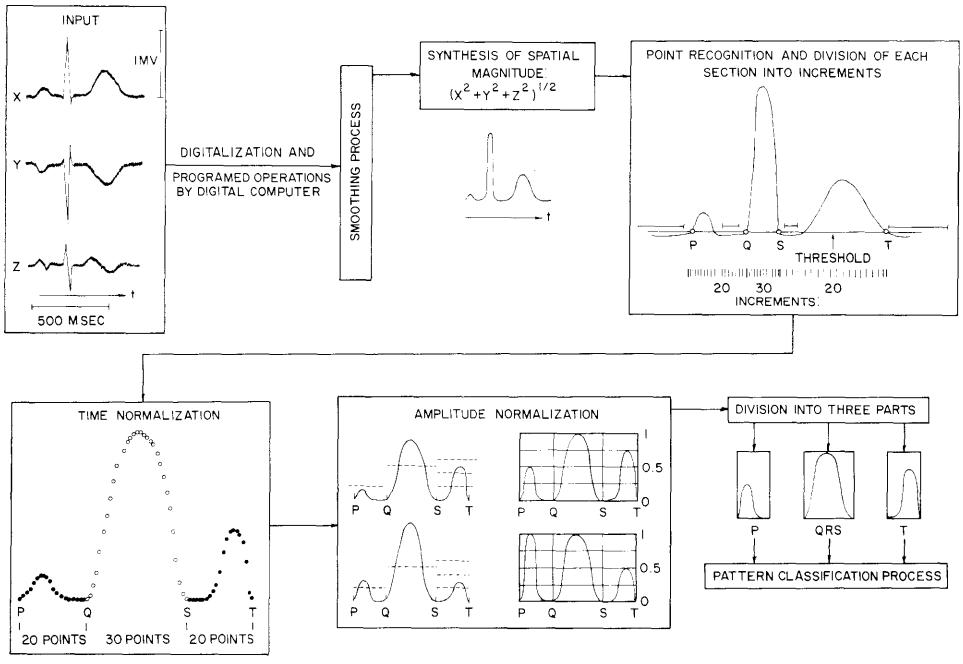

Fig. XIX-4. Point recognition, time normalization, and amplitude normalization.

by Warner and his collaborators[12] to associate EKG information with other clinical parameters.

Since the work of North,[13] matched filters have played an increasingly important role in signal detection, especially if the waveform of the signal is known, as in radar systems.[14] An adaptive matched filter modified by signal presentations to converge upon the signal waveform was studied by Glaser,[15] Jakowatz, Shuey, and White,[16] and Stark.[17] Our interest has been in the use of multiple adaptive filters that may distinguish and classify multiple signals whose crosscorrelations are high. This technique is ideally suited to high-speed digital computers because of the ease of meeting time-delay, memory, and testing requirements. It has been applied to electroencephalographic data; the following discussion will show how the method might be applied to the EKG.

Our proposed experimental data-processing system is illustrated in Figs. XIX-3 and XIX-4. The X, Y, Z components of the EKG are obtained by means of a SVEC III lead system developed by Otto Schmitt,[2,3] and are recorded on a three-channel magnetic tape system. The data are digitalized, and the magnitude of the spatial vector (MSV) is obtained in the first part of the digital program. (We use the IBM 7090 computer, and wish to express our thanks to the Computation Center, M.I.T., for their cooperation.)

A threshold level, represented by the horizontal lines (Fig. XIX-4) is set. The MSV function is required to be below this level for a required period of time indicated by the lengths of these horizontal lines. Then, any crossing by the MSV function of threshold is recorded as a sector boundary point. For example, the boundary points labelled Q and S define the QRS-complex sector. Time normalization is achieved by assigning 30 equally spaced artificial time points to the QRS sector; similarly, 20 equally spaced artificial time points are assigned to the PQ and the ST (ST-T in EKG terminology) sectors. Amplitude normalization to one of two, or one of four, levels is next performed, as shown in Figs. XIX-3 and XIX-4. The three time- and amplitude-normalized sectors (TANS) are handled separately in the adaptive pattern classification process.

The multiple adaptive matched filter was described briefly in Quarterly Progress Report No. 61 (pages 215-219). The memory filters are initially randomized as shown in Fig. XIX-5. When a data vector (one of the TANS) is presented correlation, comparison, and decision operations are performed. The memory filter that is most like the data vector is modified by the data vector. In favorable cases this process continues so that one memory filter, repetitively modified by a succession of similar data vectors, comes to resemble the data vector pattern more closely; in other words, it adapts. An example of this is shown in Fig. XIX-5, in which the third (of 20) memory filters adapts to resemble the pattern of data vector No. 1 shown in the right-hand column. Because only the memory filter with the highest correlation is modified (exclusion principle) and because there are a large number of available memory filters, different data vector patterns tend to go into different memory filters. In this way a multiple adaptive process

modifies the initially random memory filters to approach the three independent patterns of the repetitive data vectors; this adaptation is also shown in Fig. XIX-5.

The modification rule that is used most frequently is given in the program flow diagram in Fig. XIX-3. This serves to integrate the input to memory over an entire experimental run. Also shown is a smoothness of convergence rule that excludes similar, but different, patterns from a well-formed memory filter. For example, in Fig. XIX-5 data vectors No. 2 and No. 3 enter one memory filter until finally No. 2 is excluded and a new memory filter develops for it. In Quarterly Progress Report No. 61 (pages 215-219) a graphic illustration of the smoothness of convergence rule was given; in this report Fig. XIX-6 shows the results of a series of experimental runs designed to test

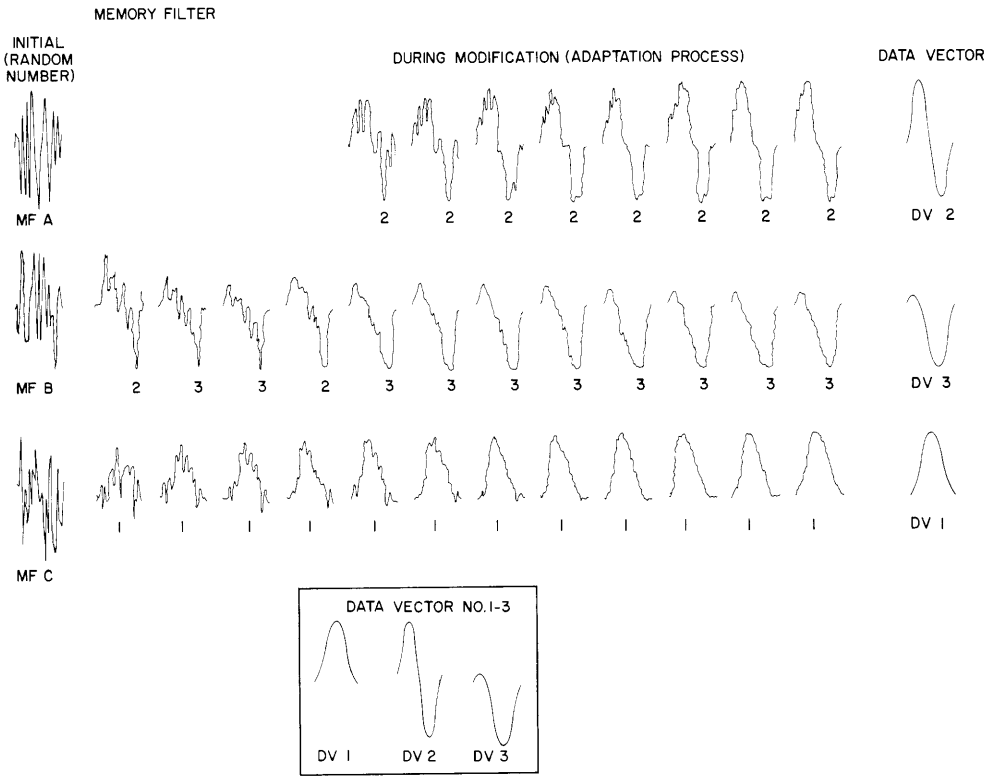

Fig. XIX-5. An example of adaptation of memory filters to repetitive presentations of data vectors. Lower trace shows how comparison and decision process assign data vector (DV) No. 1 to memory filter (MF) C on first and all subsequent occurrences. MF C becomes modified during these presentations to resemble DV No. 1. Middle trace shows that the decision process assigns both DV No. 2 and DV No. 3 to MF B at first. Eventually the convergence smoothness factor prevents DV No. 2 from entering MF B, and subsequently it enters and modifies MF A (top trace). DV No. 3 now, alone, enters and modifies MF B. Data vectors are shown at the right for comparison with their respective adaptive filters.

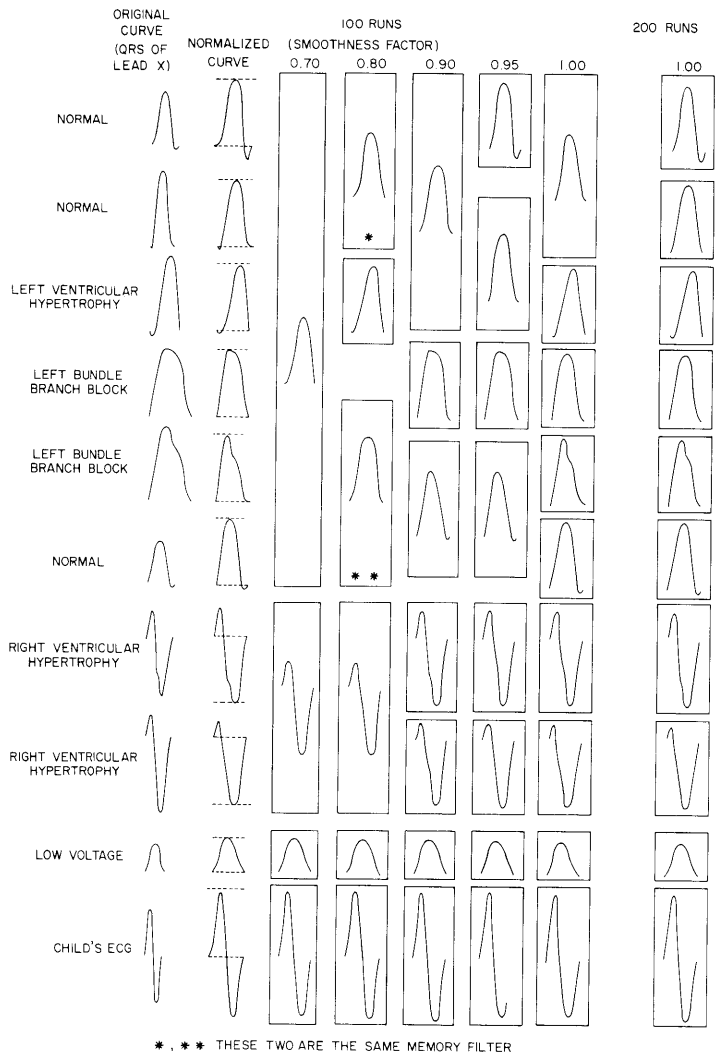

Fig. XIX-6. Results of pattern classification obtained with various settings of smoothness factor and number of presentations.

significant values of the parameter "smoothness factor" controlling this operation.

If the smoothness factor (SF) is low, then differing, but similar, patterns are accepted as identical by the program. Only quite different patterns are individually classified as unique. This is shown in the 0.70 column in which 6 of the 10 patterns are lumped, and only 4 distinct groups created. On the other hand, if SF is set to 1.0, then 8 patterns are uniquely designated and distinguished, as shown in the appropriate column of Fig. XIX-6, and only two (both variants of normal) are lumped. After an additional 100 DV presentations, even these two are distinguished.

When real data are used from different patients with the same basic electrocardiographic abnormality, the filter may be brought in the manner described above to a final

form that will pass different variations of the corresponding EKG diagnosis.

This report illustrates the background of our use of multiple adaptive matched filters that perform classifications of normalized signals. In particular, certain important aspects of the problem are discussed in detail so that the application to automatic diagnosis of clinical electrocardiograms can be understood.[18]

M. Okajima, L. Stark, G. Whipple

References

1. K. Nakagawa, Clincial studies on the orthogonal vector cardiogram using Schmitt's SVEC III lead system. 1. Normal scalar electrocardiogram, Jap. Circulation J. 23, 539 (1959).

2. O. H. Schmitt and F. Simonson, The present status of vectorcardiography, Arch. Int. Med. 96, 574 (1955).

3. O. H. Schmitt, Lead vectors and transfer impedance, Ann. New York Acad. Sci. 65, 1092 (1957).

4. H. V. Pipberger, Current status and persistent problems of electrode placement and lead systems for vectorcardiography and electrocardiography, Progr. Cardiovascular Diseases 2, 248 (1959).

5. H. V. Pipberger, E. D. Freis, L. Taback, and H. L. Mason, Preparation of electrocardiographic data for analysis by digital electronic computer, Circulation 21, 413 (1960).

6. H. V. Pipberger, R. J. Arms, and F. W. Stallman, Automatic screening of normal and abnormal electrocardiograms by means of a digital electronic computer, Proc. Soc. Exptl. Biol. Med. 106, 130 (1961).

7. F. W. Stallmann and H. V. Pipberger, Automatic recognition of electrocardiographic waves by digital computer, Circulation Res. 9, 1138 (1961).

8. M. A. Woodbury and L. D. Cady, The mathematics of pattern recognition for the electrocardiogram, a paper presented at the American Mathematical Society Symposium on Applications of Mathematics to Biology and Medicine, April 6, 1961.

9. L. D. Cady, Jr., M. A. Woodbury, L. J. Tick, and M. M. Gertler, A method for electrocardiogram wave-pattern estimation. Example: Left ventricular hypertrophy, Circulation Res. 9, 1078 (1961).

10. C. A. Steinberg, S. Abraham, and C. A. Caceres, Pattern recognition in the clinical electrocardiogram, Trans. IRE, Vol. BME-9, p. 23, 1962.

11. A. E. Rikli, W. E. Tolles, C. A. Steinberg, W. J. Carbery, A. H. Freiman, S. Abraham, and C. A. Caceres, Computer analysis of electrocardiographic measurements, Circulation 24, 643 (1961).

12. H. R. Warner, A. F. Toronto, L. G. Veasey, and R. Stephenson, A mathematical approach to medical diagnosis. Application to congenital heart disease, J. Am. Med. Assoc. 177, 177 (July 22, 1961).

13. D. O. North, Analysis of the Factors Which Determine Signal/Noise Discrimination in Radar, Report PPR-6C, RCA Laboratories, Princeton, New Jersey, June 1943.

14. G. L. Turin, An introduction to matched filters, Trans. IRE, Vol. PGIT-6, p. 311, June 1960.

15. E. M. Glaser, Signal Detection by Adaptive Filters, Technical Report No. AF-75, Johns Hopkins University Radiation Laboratory, April 1960.

16. C. V. Jakowatz, R. L. Shuey, and G. M. White, Adaptive Waveform Recognition, Report No. 60-RL-2435 E, General Electric Research Laboratory, Schenectady, New York, May 1960.

17. L. Stark, Pattern recognition for electroencephalographic diagnosis, Quarterly Progress Report No. 61, Research Laboratory of Electronics, M.I.T., April 15, 1961, pp. 215-219.

18. Dr. Gerald Whipple, Professor of Medicine, Boston University School of Medicine, together with Dr. Okajima, is supplying the clinical electrocardiographic material.

B. PREREQUISITES FOR A PHOTORECEPTOR STRUCTURE IN THE CRAYFISH TAIL GANGLION

1. Introduction

The problem of ascribing function to form is a complex and difficult one, requiring caution and critical judgment on the part of both anatomists and physiologists.[1,2] The photosensitive organ in the terminal abdominal ganglion of the crayfish has been physiologically defined only in terms of nerve-impulse response to light stimulus.[3-10] The photoreceptive structure remains unknown. Recently, a report[10] has suggested that "compound bodies which consist of a pile of lamellae, multivesicular bodies, free vesicles and dense granules, located in the innermost sheath cell of the giant fiber ... may be responsible for the light response of the ventral nerve cord of the crayfish." That this suggestion is unlikely is demonstrated by the experimental analysis in this report.

2. Method

After a routine exposure of the ventral abdominal nerve cord of the crayfish, Cambarus astacus, fine platinum electrodes mounted on a micromanipulator were applied, as illustrated in Fig. XIX-7. Careful attention to temperature, humidity, adequate blood circulation, and absence of extraneous stimulation, which is necessary for neurophysiological studies on invertebrate preparations, permitted us to work for at least six hours on a single crayfish. The light source was usually an electronically controlled glow-modulator capable of producing step changes in intensity from zero to 6 millilumens/mm^2 focussed on a π mm^2 spot.[11] This could be attenuated by means of standard neutral density filters. A brighter light source, American Optical Company's logarithmic illuminator, was used (Fig. XIX-12) for higher intensity stimuli of approximately 4.5 lumens/mm^2 over an area of 3 mm $\times$ 15 mm.

The nerve impulses, as monitored on a cathode-ray oscilloscope, are shown in Fig. XIX-7. They were also amplified, and passed to an analogue computer that generated a signal voltage proportional to the frequency of impulses. These signal voltages indicate the nerve activity that is the output of phototransduction process.

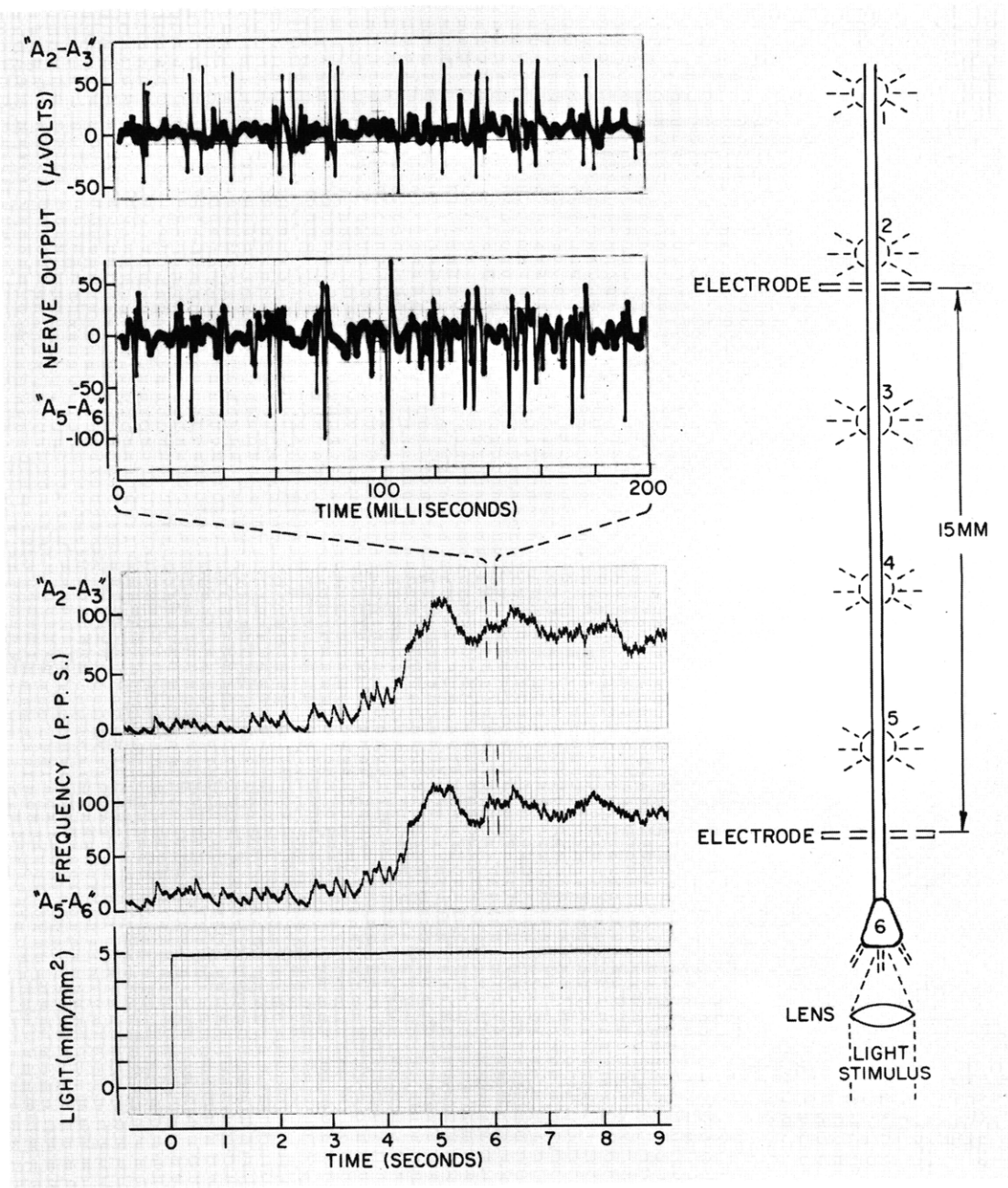

Fig. XIX-7. Experimental arrangement. Schematic diagram on right depicts relationships of ganglia and ventral nerve cord to light stimulus and electrodes. Dotted circles with adjacent numbers indicate paired ganglia (sixth is a fused double ganglion) and their characteristic triple nerve roots. Vertical double lines represent ventral cord with its enclosed B-fibers that carry light signals from caudal eye to brain centers. Two upper traces photographed from a monitoring cathode-ray oscilloscope during segment of average frequency curves (next two lower traces, demarcated by dashed lines). Letters, A2-A3 and A5-A6, denote recording electrode positions.

3. Experiment

The first experiment illustrates the well-known response of the crayfish caudal ganglion to step change of light (Fig. XIX-7). This response has served as an example of a biological transducer in more quantitative studies of both population and single unit

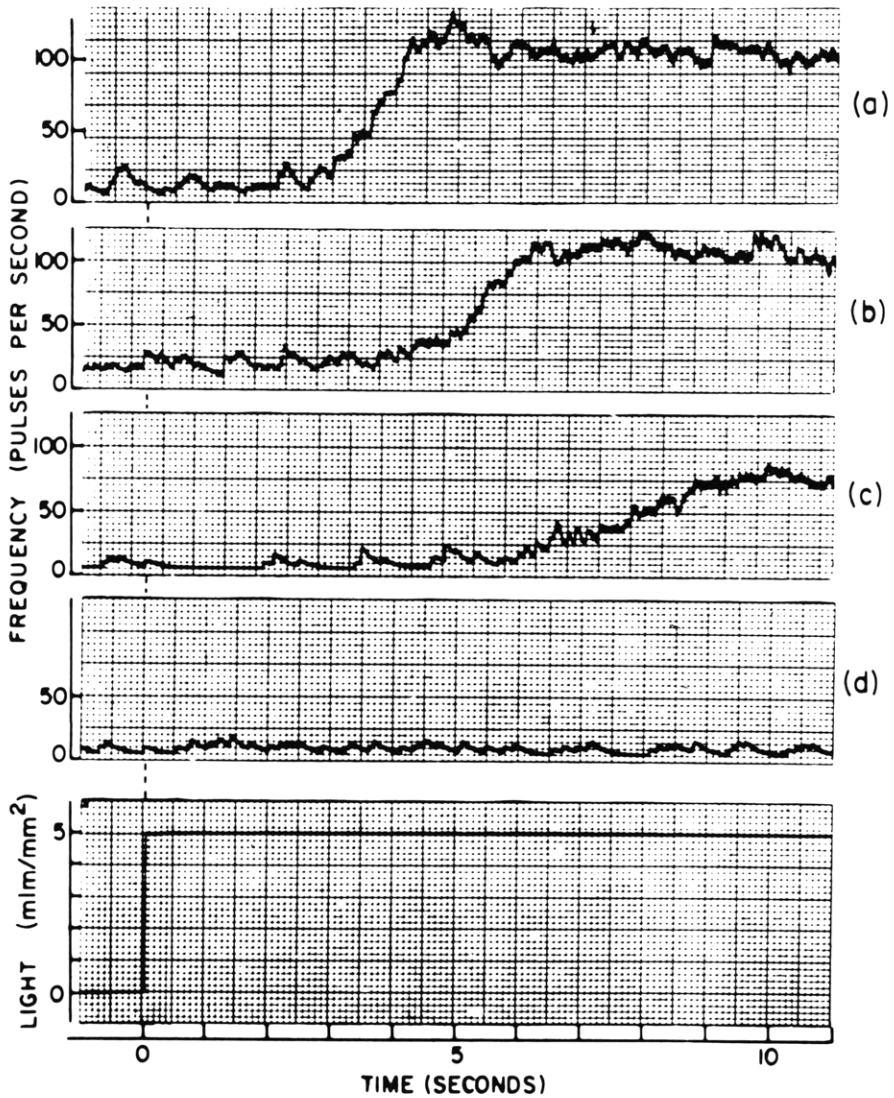

Fig. XIX-8. Light-attenuation series. (a) Trace is recorded without attenuation of 5-millilumen/mm^2 step change in light stimulus. In traces (b), (c), and (d) neutral density filters of 0.3, 0.6, and 1.0, respectively, are inserted in light path. Attenuation of (b) one-half, (c) one-quarter, and (d) one-tenth of light intensity of trace (a) results in decreasing response and increasing latency of (b) and (c). In trace (d) no response was detected (even after a minute of stimulation).

preparations. Such studies have resulted in transfer-function equations.[8, 9, 12]

The monitored nerve impulses as photographed from the cathode-ray oscilloscope were taken during the bracketed segment of the impulse-frequency curve. The relative displacements of the individual identifiable nerve impulses recorded between the fifth and sixth and between the second and third ganglia are due to the 3.8 meters per second velocity of the nerve impulses. The regularity of the displacement indicates that probably no synaptic events occurred in the three intervening ganglia. The impulse-frequency curve also shows the unchanged details of the response at the two sites of electrode placement.

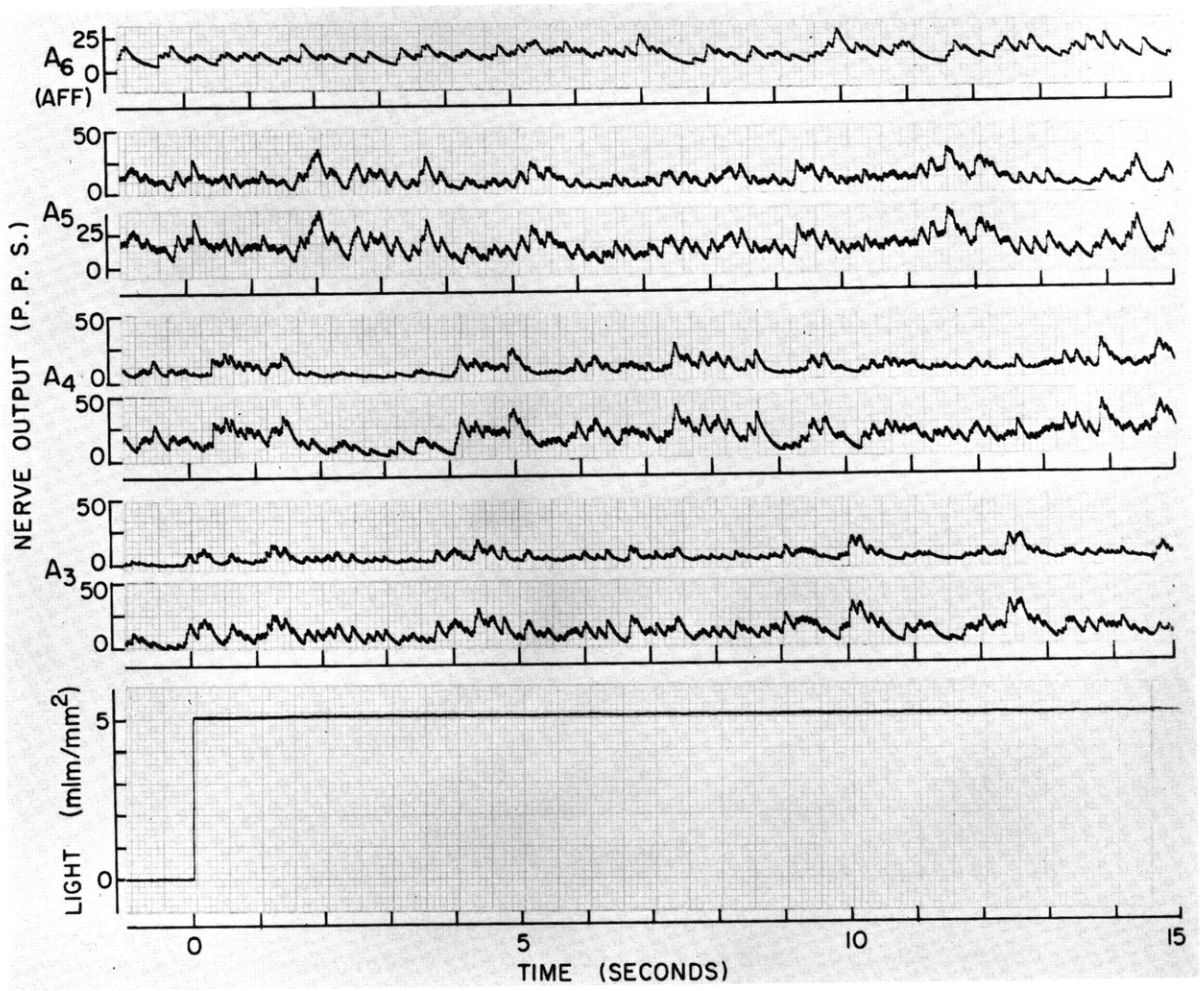

Fig. XIX-9. Response to light stimulation of ventral abdominal nerve cord and ganglia exclusive of A6. Only A6 was shielded in these experiments. In top trace, "A6 aff," nerve roots supplying A6 were stimulated. All other sites are indicated by ganglion number (A2-5) and include ganglion and adjacent nerve cord. No light response can be found anywhere.

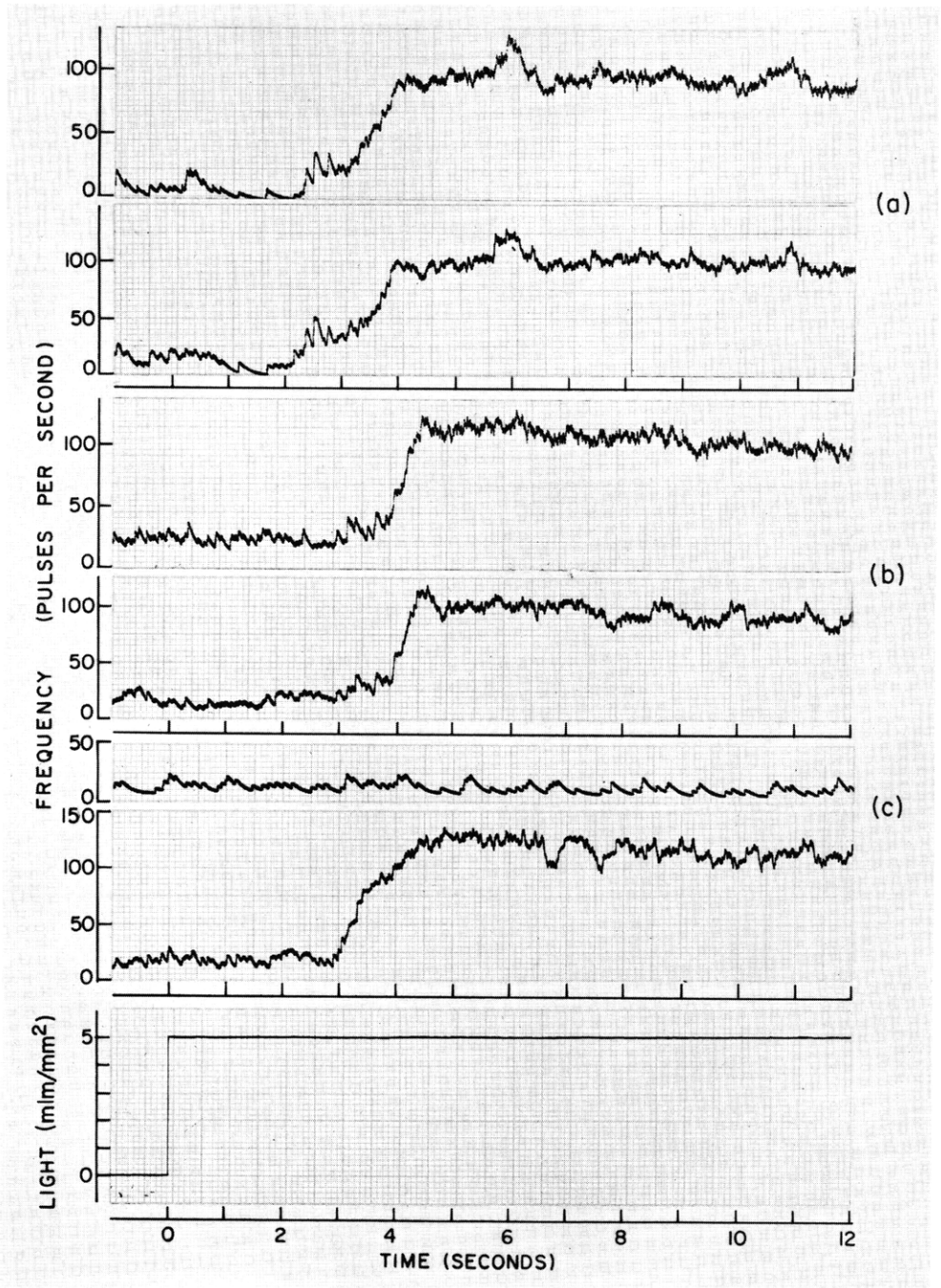

Fig. XIX-10. Transection experiments. Each pair of traces represents one experiment. Upper trace of each pair is cephalad electrode; lower, caudad electrode. (a) Control trace showing typical response to step change in light as recorded at both electrode sites. (b) All roots of A6 have been severed. No effect on light response can be seen. When in (c) cord is transected at A4-A5, light response disappears at cephalad electrode but remains unchanged in caudad electrode. Light stimulus falls on A5 and A6 only.

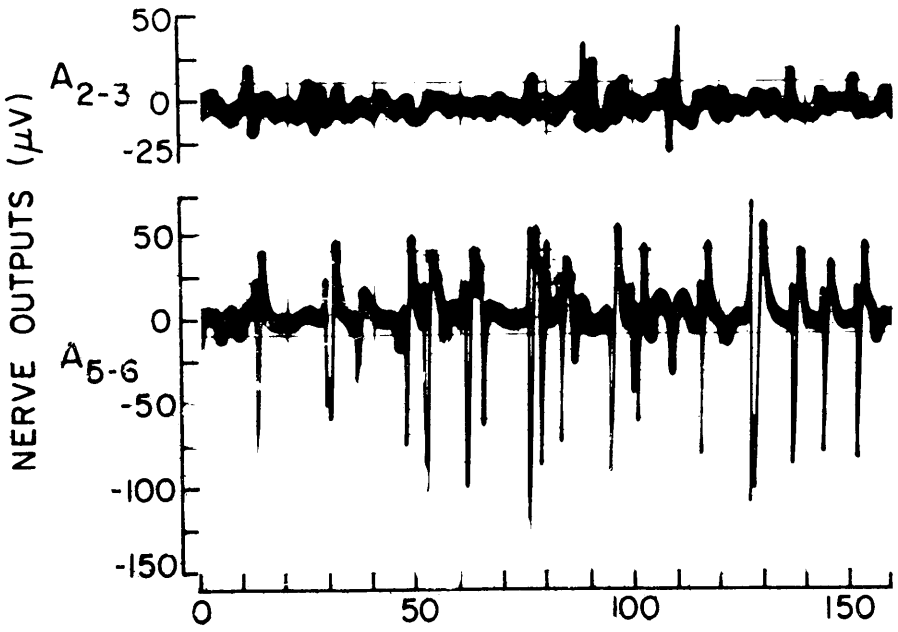

Fig. XIX-11. Photograph of monitored cathode-ray oscilloscope trace. **Top** trace recorded at cephalad electrode (corresponding to upper trace of Fig. XIX-10c). Photograph taken after rise had reached its steady level. Lower trace is caudad-electrode recording of B-fiber activity, emanating from A6 ganglion. (Only small C-fiber activity can be seen.)

The increase in frequency of nerve impulses that carries the light signal is more conveniently displayed by the nerve impulse-frequency curve. Thus, in the following experiments, we relied primarily on this graphic display of photoreceptor activity.

By suitable choice of neutral density filters, we attenuated the stimulus flux, and the response of the sixth abdominal ganglion was accordingly changed as shown in Fig. XIX-8. The photoreceptor response, although reduced and delayed, is still in evidence at one-fourth the level of the original stimulus flux. However, when the stimulus light was focussed on the sixth ganglion nerve roots, containing both afferent and efferent nerve fibers, or on the other abdominal ganglia, no response was evident, as shown in Fig. XIX-9. This was also true for any part of the ventral abdominal nerve cord in the interganglionic regions. Furthermore, even light sources of three-hundredfold maximum glow-modulator intensity produced no effect in any abdominal or tail structure, except in the sixth ganglion.

A further experimental demonstration that only the sixth ganglion produces nerve impulses in response to light may be seen in Fig. XIX-10. Here are shown: (a) the normal response; (b) the response negligibly altered after transection of the nerve roots of the sixth ganglion; and (c) the nerve impulses emanating from the sixth ganglion, which are noted only in the caudad electrode when the ventral nerve cord is transected

just below the fifth ganglion. The monitored trace of the raw-nerve-impulse trains, from both the sixth and the third ganglia, in the experimental situation of Fig. XIX-10c, are shown in Fig. XIX-11. The light-response impulses are of moderate amplitude, as opposed to the small spontaneous impulses (which, of course, are not excluded from the cephalad electrode).

However, it is necessary to recall that the crayfish has an extremely well-developed

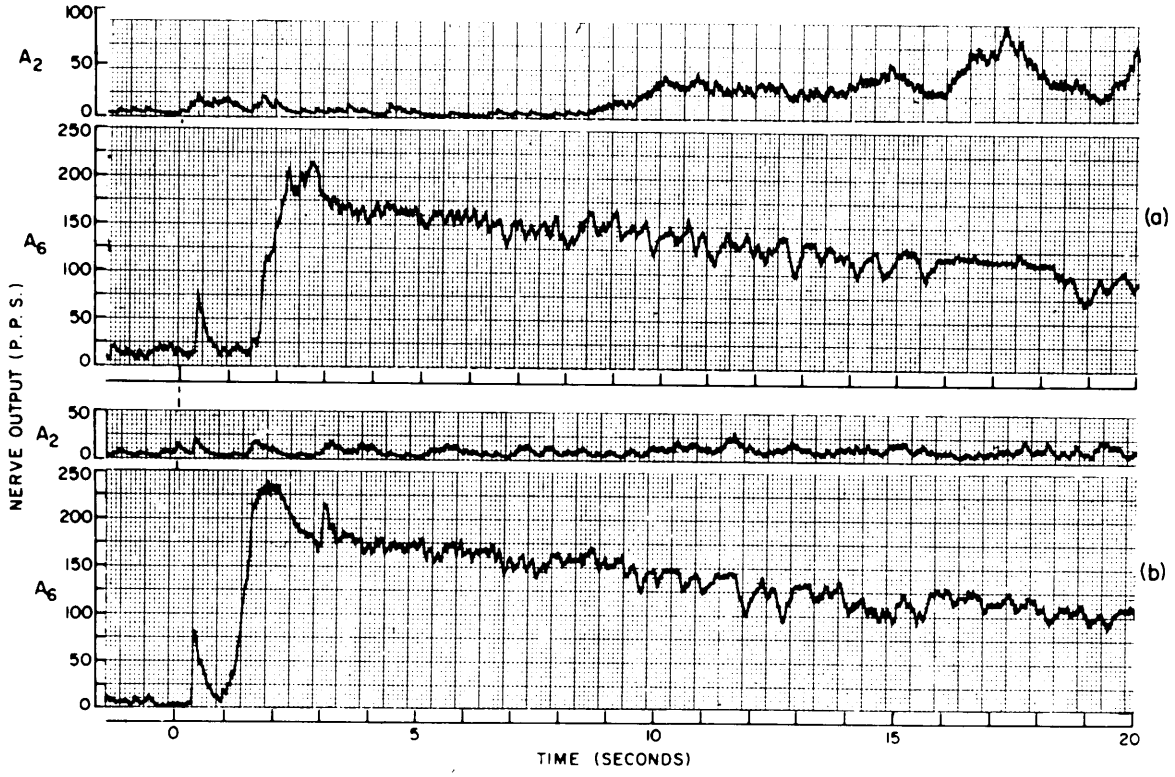

Fig. XIX-12. High-intensity light experiment. Light intensity of 4500 lumens/mm^2 was employed to stimulate entire nerve cord under study. Upper and lower trace of each pair represents cephalad and caudad electrodes. (a) Cord was transected between A4 and A5. Small, sharp, early response, detected a few hundred milliseconds after stimulation, is found only in high-intensity stimulation. Early response resembles in frequency and form the rapidly adapting "on" response recorded from cephalic eye single units of crayfish. The main response rising rapidly 1 sec after stimulation dwarfs early response. Response overshoot magnitude, and ac adaptation are characteristic of very large step changes in light. Approximately 10 sec after onset of light an anomalous late response appears at the A2-A3 recording site. Since cord has been transected at A4-A5, it cannot originate in A6 ganglion. (b) Same preparation with cord also transected between A1 and A2. Upper trace is cephalad electrode, recording at the A2-A3 interval; lower trace, caudad electrode at A5-A6. No response seen in cephalad electrode. It is clear that anomalous late response was due to stimulation of elements cephalad to A2. Very likely cephalic eyes, picking up scattered light, are responding.

and sensitive pair of cephalic eyes, capable of complex visual information processing. When extremely high intensity light stimuli impinge diffusely on a 3 mm × 15 mm area of the crayfish abdomen, illuminating the entire chain of ganglia, some response mediated by means of these cephalic eyes is only to be expected (from scattering in the experimental chamber). The experiment illustrated in Fig. XIX-12 shows a careful control of this factor. In a manner similar to that of the preceding experiment, the cord is cut just caudad to the fifth ganglion. The light-response nerve impulses from the sixth ganglion can reach only the caudad electrodes. However, the cephalad electrode picks up a long-latency, slowly rising anomalous response. When the nerve cord is transected cephalad to the second abdominal ganglion, this anomalous response is eliminated. Thus it is attributable to a response to scattered light, mediated by the cephalic eyes.

4. Discussion

It is necessary, first, to assemble the relevant physiological arguments concerning the photoreceptor. The sixth abdominal ganglion appears to be the only locus of visual excitation in the ventral abdominal nerve cord. Other workers so indicate, and our experiments, especially designed to elucidate this point, clearly establish it. Any photoreceptor must have a sensitivity a thousand times less than that of the sixth ganglion and, furthermore, must not generate identifiable nerve impulses.

The nerve impulses signalling the light stimulation are carried by the B-fibers only.[8] The B-fibers occupy a medium range in the nerve-impulse-height spectrum; this point also has been confirmed by nerve conduction velocity studies. The A-fibers, which produce greater pulse heights, show no activity that is correlated with light stimulus, and the small C-fibers actually show a negative correlation with light. In addition, the giant fibers can be removed by dissection without interference with the light response of the B-fibers. Furthermore, by careful quantitative measurement of the dynamic characteristics of the tail ganglion photoreceptor organ, we have been able to prove that only two to four B-fibers contribute to the population response. Single fiber studies by ourselves[13] and others[7] confirm this.

To summarize these arguments, nerve impulses are generated in the sixth ganglion itself, and conducted by means of from two to four B-fibers through the ventral nerve cord.

It is unfortunate that the exact locus of the photoreceptor organ is unknown. Kennedy and Preston found only two light units after extensive probing with microelectrodes inside the ganglion. The extreme difficulty of such a search may be expected from the ratio (~4:2000) of light-sensitive to other neurons – if indeed the light-sensitive structure is a neuron. The photo pigment has, of course, still not been extracted, although it has spectral characteristics that are identical to rhodopsin.[14] These shortcomings are due, in part, to the present limited physiological definition of the photoreceptor organ in

terms of nerve-impulse response.

In view of the defined experimental criteria and the lack of precise locus we turn toward anatomical evidence concerning the photoreceptor organ. Hama recently described[11] "a structure which resembles closely known types of photoreceptors in animals and plants has been detected in the abdominal ganglions of the crayfish."

On two physiological grounds these structures cannot be related to the photoreceptor organ in the sixth abdominal ganglion. First, they are not restricted to the sixth ganglion as is the photosensitivity. Second, he states that they are associated with the giant-fiber system and not with those few B-fibers that uniquely carry the photoresponsive nerve impulse signals.

How secure is Hama in reasoning from evidence of similarity in form? The main characteristic of these "compound bodies" seems to be the parallel lamellae so common in submicroscopic organelles. Indeed, myelin sheath, mitochondria, and vertebrate rod and cone outer segments alike show exquisite lamellate morphology.[15, 16] However, rhabdomes that are characteristic of invertebrate eyes do not show lamellae, but rather a complex, tubular, honeycombed structure, less tightly packed and ordered than in the more primitive photosensitive organs such as the simple eye of the spider.[17-22] We therefore must reject even the anatomical argument based upon structural analogy.

The extremely primitive nature of the photoreceptor organ of the crayfish tail ganglion, without optical apparatus or spatial array, naturally invites careful exploration of this interesting area with the electron microscope and other anatomical tools. However, the anatomist must be guided by the physiological definition of the elusive structure he is seeking.

Physiological investigation has restricted the crayfish tail photoreceptor organ to include photosensitive elements lying only within the sixth abdominal ganglion, and from two to four B-fibers carrying nerve-impulse responses through the ventral nerve cord. It is therefore possible to exclude the "compound bodies"[10] associated with the giant-fiber system, and located diffusely in the nerve cord, from any role in the phototransduction process. Attention of anatomists is called to this primitive and interesting photoreceptor organ.

H. T. Hermann, L. Stark

References

1. S. Cobb, Observations on the comparative anatomy of the Avian brain, Perspectives in Biology and Medicine, Vol. III, 1960.

2. H. Lamport, A. Mauro, and L. Stark, How is tension transmitted from striated muscle fiber to tendon? Abstracts of Communications – 20th International Physiological Congress, Brussels, July 1956.

3. C. L. Prosser, Action potentials in the nervous system of the crayfish. II. Response to illumination of the eye and caudal ganglion, J. Cell. Comp. Physiol. 4, 363 (1934).

4. J. H. Welsh, The caudal photoreceptor and responses of the crayfish to light, J. Cell. Comp. Physiol. 4, 379 (1934).

5. C. A. G. Wiersema, S. H. Ripley, and E. Christensen, The central representation of sensory stimulation in the crayfish, J. Cell. Comp. Physiol. 46, 307 (1955).

6. D. Kennedy, Responses from the crayfish caudal photoreceptor, Am. J. Ophthalmol. 46 (Part II), 19-26 (1958).

7. D. Kennedy and J. B. Preston, Activity patterns of interneurones in the caudal ganglion of the crayfish, J. Gen. Physiol. 43, 655 (1960).

8. L. Stark and H. T. Hermann, The transfer function of a photoreceptor organ, Kybernetik 1, 124-129 (1961).

9. L. Stark and H. T. Hermann, Light transfer function of a biological photoreceptor, Nature 191, 1173 (1961).

10. K. Hama, A photoreceptor-like structure (ventral) nerve, Anat. Record, pp. 329-336, 1961.

11. L. Stark, Stability, oscillations, and noise in the human pupil servomechanism, Proc. IRE 47, 1925-1939 (1959).

12. L. Stark, Transfer Function of a Biological Photoreceptor, WADC Technical Report 59-311, August 1959, pp. 1-22.

13. H. T. Hermann, L. Stark, and P. A. Willis, Instrumentation for processing neural signals, EEG Clin. Neurophysiol. (in press).

14. W. R. Utal and Hedwig Kaspr Zak, Caudal photoreceptor of crayfish adaptation and luminosity function, Abstracts of the Biophysical Society Meeting, February 1962.

15. F. S. Sjostrand, The ustrastructure of the retinal receptors of the vertebrate eye, Ergeb. Biol. 21, 128 (1959).

16. J. D. Robertson, The molecular structure and contact relationships of cell membranes, Progr. Biophys. 10, 343-418 (1960).

17. W. H. Miller, Morphology of the Ommatidia of the compound eye of Limulus, J. Biophys. Biochem. Cytol. 3, 421 (1957).

18. T. H. Goldsmith and O. E. Philpott, Microstructure of the compound eyes of insects, J. Biophys. Biochem. Cytol. 3, 429 (1957).

19. H. Fernandez-Moran, Fine structure of the light receptors in the compound eyes of insects, Exptl. Cell Res. Suppl. 5, p. 586, 1958.

20. J. J. Wolken, J. Capenos, and A. Turano, Photoreceptor structures. III. Drosophila Melanogaster, J. Biophys. Biochem. Cytol. 3, 441 (1957).

21. J. J. Wolken, Retinal structure. Mollusc Cephalopods: Octopus, Sepia, J. Biophys. Biochem. Cytol. 4, 835 (1958).

22. M. F. Moody and J. D. Robertson, The fine structure of some retinal photoreceptors, J. Biophys. Biochem. Cytol. 7 (Part 1), 87-91 (1960).

C. EXPERIMENTS ON THE VISUAL SYSTEM OF THE LAND CRAB

An investigation of the visual system of the land crab was undertaken in Puerto Rico[1] to complement the studies on the human visual system which are being performed at the Research Laboratory of Electronics. The land crab was chosen as the experimental animal that would most fruitfully lend itself to a comparative study of this kind. The

class of crustacea, although it has a visual system that is nearly as highly developed as that of vertebrates, has a nervous system composed of readily defined ganglia that allow the experimenter to record system activity step by step through the neurological processes. Among crustacea, the land crab was chosen, rather than the readily available crayfish because its normal environment is dry land, and its eyestalks are rather large and fully retractable – to simplify the experimental conditions.

The research consisted of two portions. In the first, a study was made of optokinetic nystagmus in the crab; in the second portion, macroelectrode recordings were taken from many points on the animal in order to indicate those areas from which the most useful information on visual stimulation could be obtained.

1. Compensatory Movements and Nystagmus

(a) When the crab is held in its normal orientation and rotated slightly, the eyestalks compensate by moving in the opposite direction to maintain a stabilized visual field. After some time, presumably, the eyestalks revert to their central position.

(b) When the crab is rotated at a constant rate about a vertical axis, and the surrounding field is either the laboratory or a drum with several contrasting vertical stripes, the eyestalks move in a manner that is typical of optokinetic nystagmus. The slow movement is always compensatory, and the fast jerk is in the direction of rotation of the animal. The jerks occur simultaneously in the two eyestalks, although the leading eye seems to predominate in triggering the jerks. The frequency of jerks is dependent upon the rate of rotation and the inhomogeneity of the surrounding field. For fast rotations (greater than 9 degrees per second) the interval between jerks seems to be a relatively constant time interval (2-5 sec) rather than a constant angular displacement. For slower rotations, and a sufficiently inhomogeneous visual field, the jerks occur approximately every 30° of field rotation.

Data showing the average time between jerks and angle between jerks are given in Fig. XIX-13a and -13b. For high-speed rotations (greater than 50 degrees per second) the eyestalks either withdraw or remain stationary. The solid lines in Fig. XIX-13 indicate the asymptotic predicted values of average time and angle between jerks. In region a, for rotations slower than 9 degrees per second, the lines indicate a return jerk for every 27° of rotation. In region b (9-50 degrees per second), the asymptotes are constant for a time interval of 3 seconds between jerks. Region c indicates that for rotations faster than 50 degrees per second the nystagmus effect disappears, with the time and angle between jerks going to infinity.

(c) When the external field (drum) is rotated with the crab, the nystagmus is eliminated in the steady state; this indicates that a movement of the crab relative to the visual field is necessary for this optokinetic nystagmus.

(d) When the crab is stationary and the drum is rotated, a pattern of nystagmus is

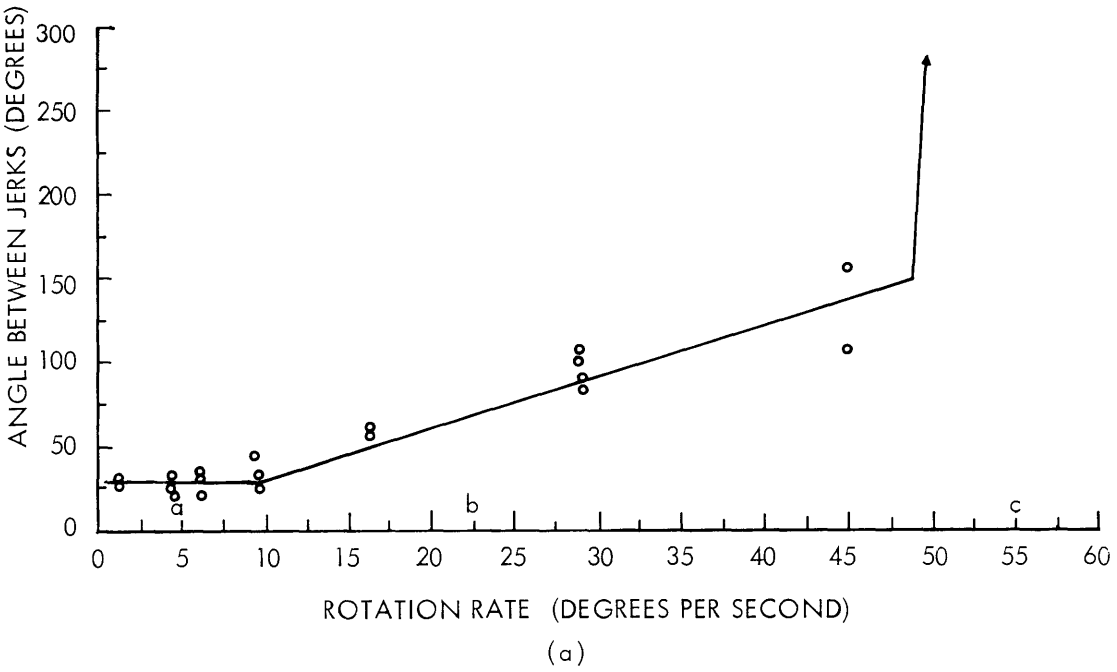

(a)

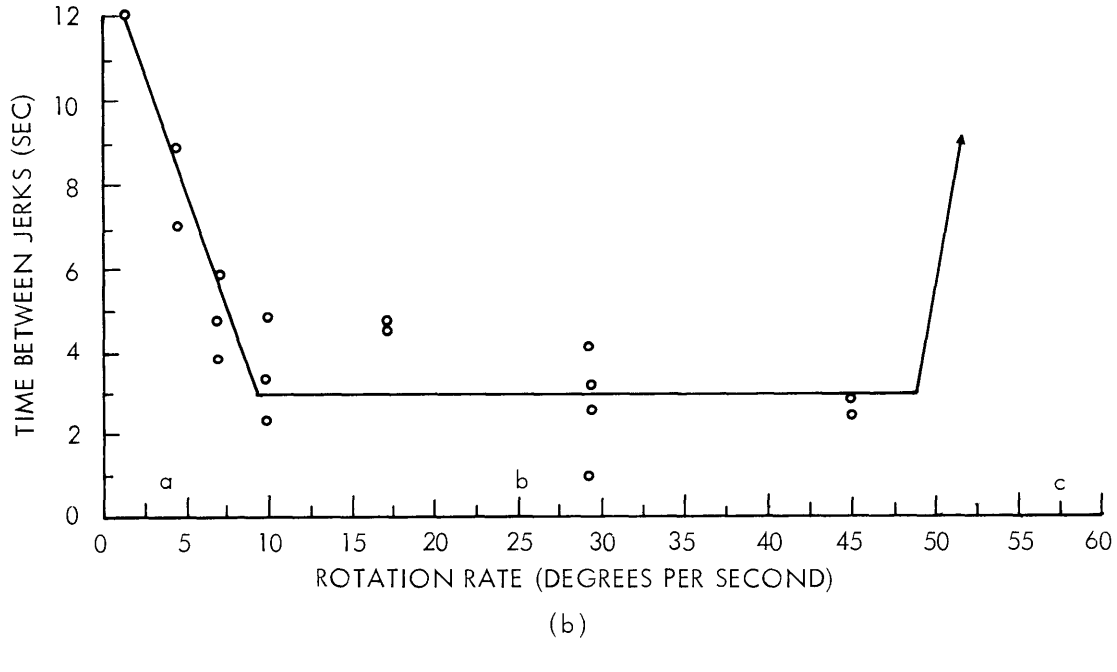

(b)

Fig. XIX-13. (a) Average angle and (b) time between fast phases of nystagmus.

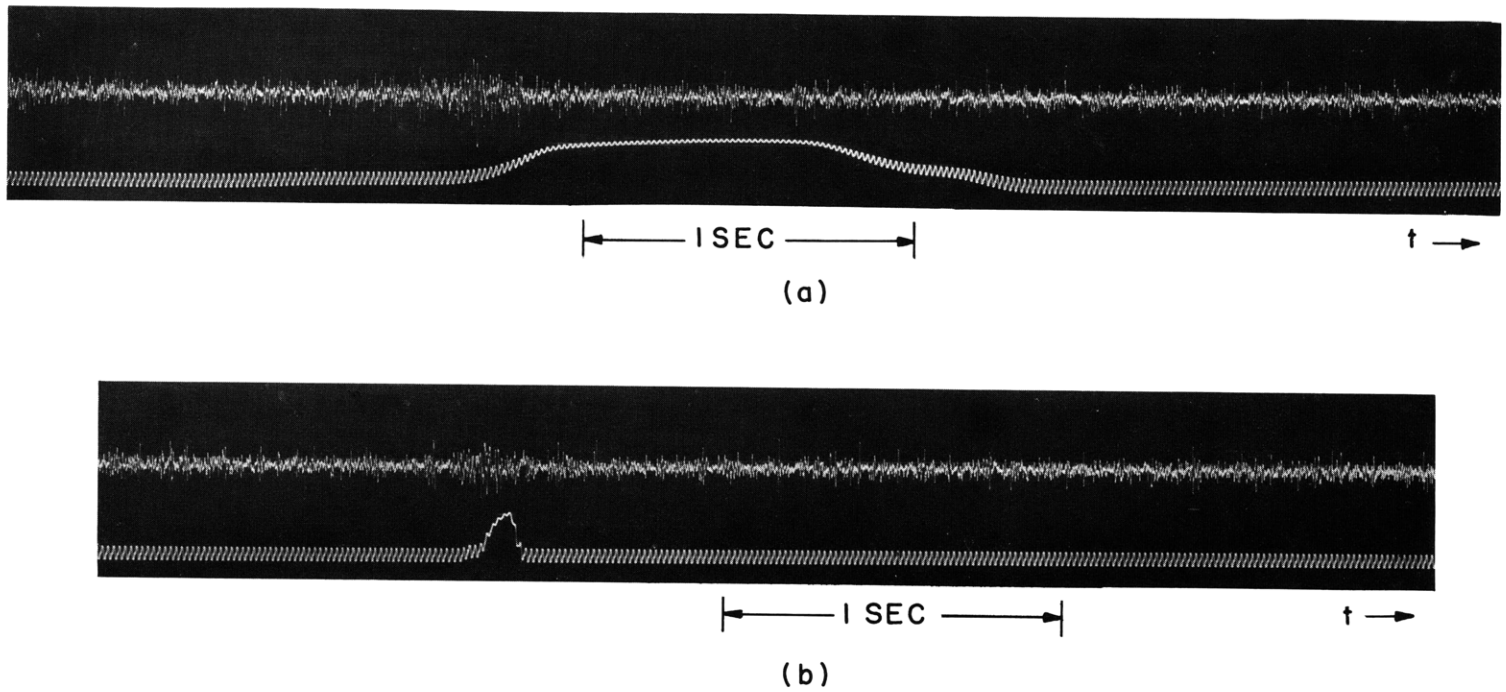

Fig. XIX-14. Electrical measure of visual activity.

observed which is similar to that noted during rotation of the animal with respect to its field.

The nystagmus effect is maximal for the greatest inhomogeneity of the moving visual field (the condition with no surrounding drum). The nystagmus rates are diminished when the crab is rotated inside a drum with six black-white vertical boundaries, still further diminished when the number of boundaries is reduced to three, and virtually eliminated when the drum is of uniform color.

2. Electrode Recordings

All recordings were made with silver or platinum macroelectrodes recording differentially from two areas on the crab, with the underside of the shell of the crab grounded.

(a) "On" response. With differential recording from one eye, ~4 mm from the end of the eyestalk, an increase in the frequency and amplitude of the recorded pulses was observed when the ambient light was increased. The activity subsided with a time constant of 2-4 seconds.

(b) Response to moving stimulus. Recordings were taken from two loops of silver wire, which were wound around the basal segment of each eyestalk. A burst of high-amplitude impulses, characteristic of unit nerve firings, appeared every time an object moved into the visual field. Recordings of this type are shown in the upper traces of Fig. XIX-14. The lower trace is the output of a small photocell positioned near the crab. This figure shows the visual activity stimulated by the approach of a human hand. The width of the photocell spike indicates the speed of approach of a (4-inch) human hand. Notice that the increased activity in Fig. XIX-14 started when the hand moved into the animal's field of view, and before passing directly over the crab. This measure of visual activity indicated a response to any movement in the visual field of the crab. It could be induced by throwing a small object across the cage, or by having the experimenter shift position in his chair, six feet away.

L. R. Young

References

1. This research was performed in the laboratory of Dr. José del Castillo, Professor and Head, Department of Pharmacology, School of Medicine, University of Puerto Rico, San Juan, Puerto Rico, under Air Force Contract AF49(638)-1130. The author expresses his appreciation to Dr. Lawrence Stark who arranged the exchange, and to Dr. del Castillo, who proposed this study, and throughout the investigation was of invaluable aid through his guidance and collaboration.

D. PUPIL RESPONSE TO SHORT-DURATION PULSES

Since the development of quantitative pupillography, several attempts have been made to analytically formulate the pupil system for response to light. Our approach

follows the servoanalytic model[1] because of its generality and flexibility. The assumption in this model is that the system is linear in the range of operation, and, by a straightforward application of the ideas of circuit analysis to amplitude-phase versus frequency data, a model for the system is deduced. This model consists of three equal lag elements described by the system transfer function.

In a review elaborating this viewpoint nonlinear operators were proposed which undoubtedly played a role in shaping the pupillary response under normal operating conditions.[2] Two such nonlinearities are of particular importance and are operative in normal vision: (a) In initial elements of the system, there is a considerable scale compression that is often characterized by physiologists as a log operator. (b) Biological sensory systems frequently become less sensitive to a constant stimulus over a period of time and such time-dependent insensitivity in the visual system has been termed light and dark adaptation. Therefore, the early model was superseded by one that could be characterized by a block diagram consisting of three series elements relating flux-in to area-out, and the signal flow was: light flux → log operator → adaptation → lag elements → area. The flow diagram was based, in part, on neurophysiological evidence that indicates scale compression in the retina and evidence previously given[3] which places the integrating elements in the iris muscles.

Previously, work on this model was based primarily on steady-state sinusoidal data. In this report we attempt to bring together the model and transient data, primarily responses to short-duration pulses. Since pulse widths were much less than time constants of retinal adaptation, the adaptation operator may be eliminated from consideration in this analysis. The model transfer function therefore has the form

$$\Delta A = a \log F\, W(\tau), \tag{1}$$

where a is some constant, and $W(\tau)$ is a function of the pulse width τ only.

1. Methods

The basic instrumentation and methods for stimulating the retina and measuring the pupil area have been previously outlined.[4] Also, stimulating equipment was modified to generate pulses with a rise-time constant of 10 μsec from zero initial flux.

Subjects were dark-adapted for 5 minutes after positioning in the pupillometer. Experimental runs consisted of pulses of light presented every 15 sec, and experimental designs were arranged in a Latin square; the experimental values presented here are averages of the replications. The parameters that were varied are pulsewidth and pulse height; the variation was 1-100 msec for the former, and 10^{-3}-1 millilumen for the latter. Preliminary investigations demonstrated that 15 seconds between trials was sufficient to eliminate interaction.

2. Results

(a) The shape of a typical pulse response to a 1-msec pulse of (ND2) lumens is shown in Fig. XIX-15 and compared with impulse responses of second-, third-, and fourth-order systems composed of equal lags that were adjusted to make peak responses coincide. Of interest is the long time to peak compared with input pulsewidth and the close approximation to a third-order response.

(b) The dependency of peak amplitude of response on light flux has been shown to be linear with log flux for fluxes of (ND3) to (ND0) lumens and pulse durations of 1-100 msec. An experiment conducted by using pulse durations of 10 msec is illustrated in Fig. XIX-16. Although these results correspond well with the predictions of the model in question, if the amplitude-dependent, no-memory operator precedes the memory elements, then the ratio

$$\frac{\Delta A(\tau_1, F_1)}{\Delta A(\tau_1, F_2)} = \frac{\Delta A(\tau_2, F_1)}{\Delta A(\tau_2, F_2)} = \frac{\log F_1}{\log F_2} \tag{2}$$

should be independent of pulsewidth. That this is not so has been deduced from an experiment in which there were four stimulating conditions with durations of 1 msec and 100 msec, and with fluxes of (ND2) and (ND0) lumens. The results are given in Table XIX-1 and Eqs. 3 and 4.

Table XIX-1. Experimental results.

τ; F	1; 10^{-2} m.l.	1; 1 m.l.	100; 10^{-2} m.l.	100; 1 m.l.
ΔA	5.25	11	9.5	14

$$\frac{\Delta A(1; 1)}{\Delta A(1; 10^{-2})} = 2 \tag{3}$$

$$\frac{\Delta A(100; 1)}{\Delta A(100; 10^{-2})} = 1.5 \tag{4}$$

(c) The response as a function of pulsewidth is illustrated in Fig. XIX-17. An experiment was run at three different light fluxes. Pulse durations were varied from 1 to 100 msec. It is interesting that amplitude of response falls off only at very short durations compared with response time to peak. In linear systems pulses that are short by an order of magnitude compared with system response time produce responses that are proportional to the pulsewidth. It is obvious that the data of Fig. XIX-17 do not fit such an interpretation. It is instructive to compare the pusle-amplitude dependence

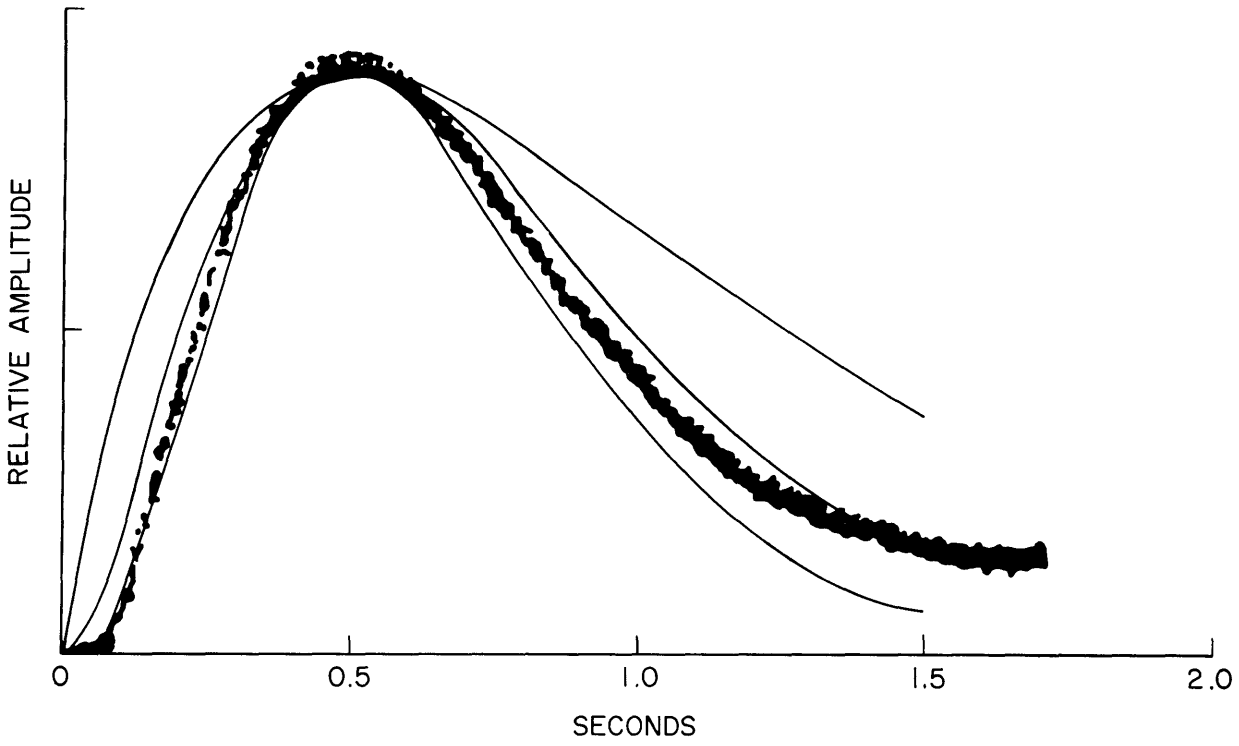

Fig. XIX-15. Pupil response compared with impulse response of second-, third-, and fourth-order systems.

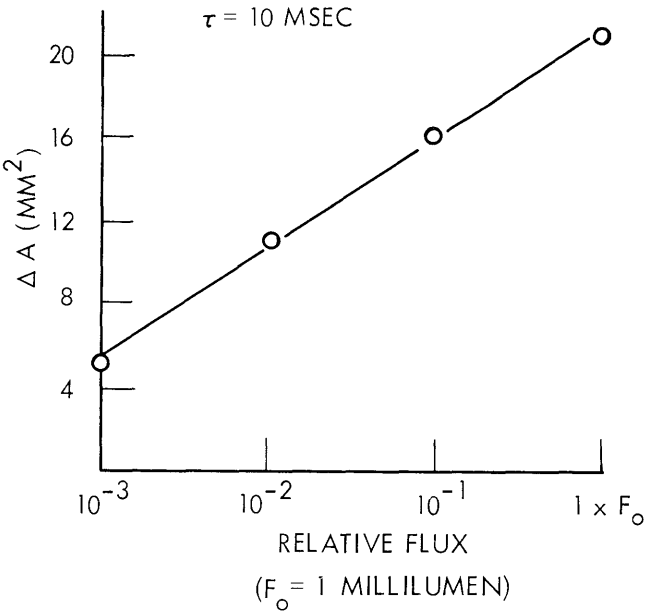

Fig. XIX-16. Maximum amplitude of response as a function of input flux. Pulse duration, 10 msec.

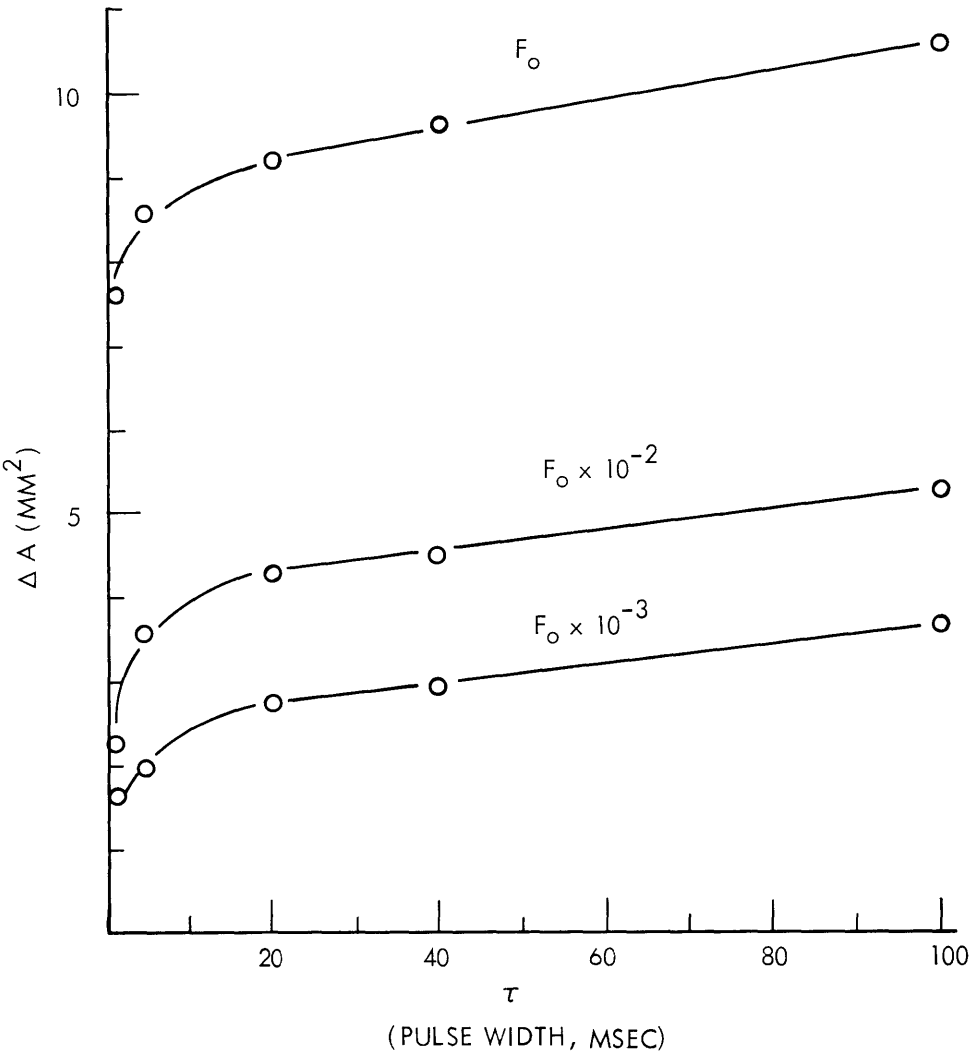

Fig. XIX-17. Maximum amplitude of response as a function of pulsewidth for three different fluxes (F_o = 1 milliumen).

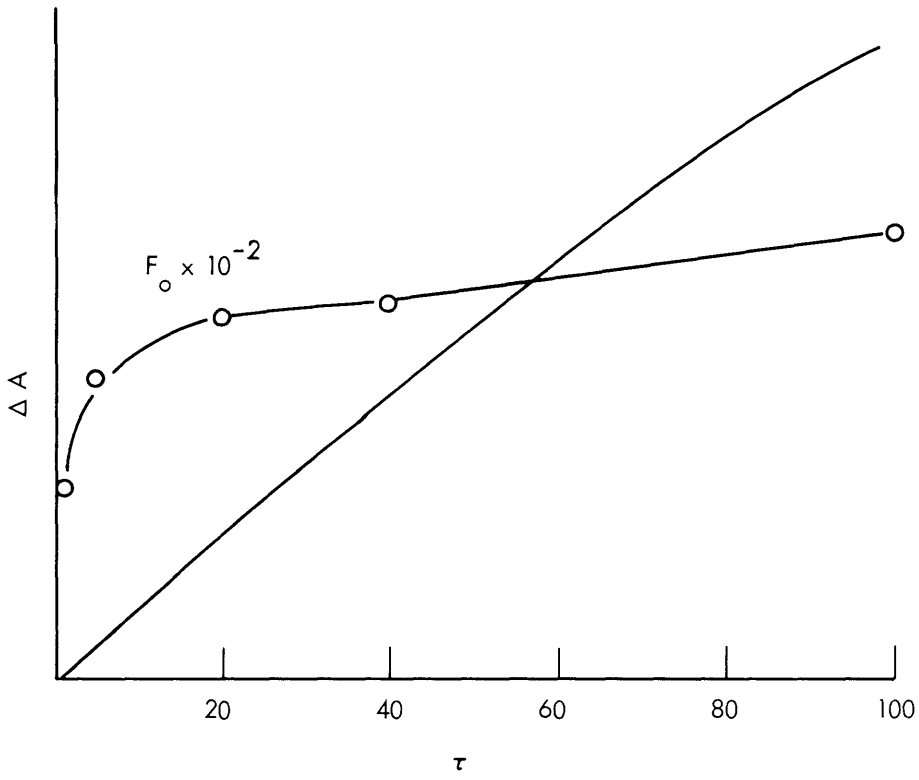

Fig. XIX-18. Pupil system compared with ideal third-order system with respect to dependency on pulsewidths that are short compared with time constants.

of the pupil system with an ideal analogue (with the same times to peak) such as the third-order system illustrated in Fig. XIX-15. That the shapes of the two differ markedly, as illustrated in Fig. XIX-18, indicates a nonsuperposition of the responses to time-distributed inputs.

3. Discussion

This study reveals that under the present conditions of operation the pupil system has a response to short-duration inputs which resembles the impulse response of a third-order system and has a log input-intensity dependency at any given pulsewidth. Although these relationships are in agreement with the predictions of the above-mentioned model, a log operator placed at the beginning of the system has been shown to be insufficient to account for data of response as a function of pulsewidth. This fact is in keeping with certain neurophysiological evidence,[5] in which integration has been noted early in the visual process. Also, it is easily demonstrated that a pupil response elicited by stimulation of both eyes together is not the sum of the responses of each eye stimulated separately, if in all instances the response of a single pupil is measured.

Therefore, some saturation takes place at or after summation of retinal signals in the mesencephalon.

This report reveals that assumptions in the three-block model are not completely applicable under the operating conditions used here. Although these conditions simplify the handling of certain analytical problems, for instance, ambiguities of states of retinal adaptation or ignorance of the neuromuscular transfer function, the system was operated in a state of maximum gain and therefore flux changes that might be small under sinusoidal steady-state conditions might be large under the conditions of our experiments. Thus caution must be exercised in using these results for interpreting other data.

F. H. Baker

References

1. L. Stark and P. M. Sherman, A servoanalytic study of the consensual pupil reflex to light, J. Neurophysiol. 20, 17-26 (1957).

2. L. Stark, Stability, oscillations, and noise in the human pupil servomechanism, Proc. IRE 47, 1925-1939 (1959).

3. L. Stark and F. H. Baker, Stability and oscillations in a neurological servomechanism, J. Neurophysiol. 22, 156-164 (1959).

4. L. G. Bishop, Julia H. Redhead, and L. Stark, Servoanalysis of the pupil of the owl, Quarterly Progress Report No. 63, Research Laboratory of Electronics, M.I.T., October 15, 1961, pp. 193-204.

5. H. K. Hartline, Intensity and duration in the excitation of single photoreceptor units, J. Cell. Comp. Physiol. 5, 229 (1934).

E. PULSE RESPONSE OF THE PUPIL

Responses of a linear system to pulses (whose duration is short with respect to the response dynamics) should show a constant time to peak; different areas of input pulse should result in differing response heights following the law of superposition. Sparse experimental data suggested that the pupil system might show this constant time to peak,[1] but it was felt that more adequate study was necessary. The present experiments were designed to test this hypothesis.

The organization of an experiment is shown in Fig. XIX-19. A broad range of pulse-widths was selected in which the widest pulses exceeded the constraint mentioned parenthetically above. The pulse heights were selected in order to obtain a reversed diagonal of approximately equal response heights. In order to eliminate trend effects, the nine combinations of stimuli parameters were arranged in a Latin-greco square; pulses were applied every 4 seconds. Average values of response amplitude and time to peak are plotted in Fig. XIX-20 as a function of stimulus pulse energy. It is clear that both measures of pupil response change with stimulus energy. In Fig. XIX-21 is shown the

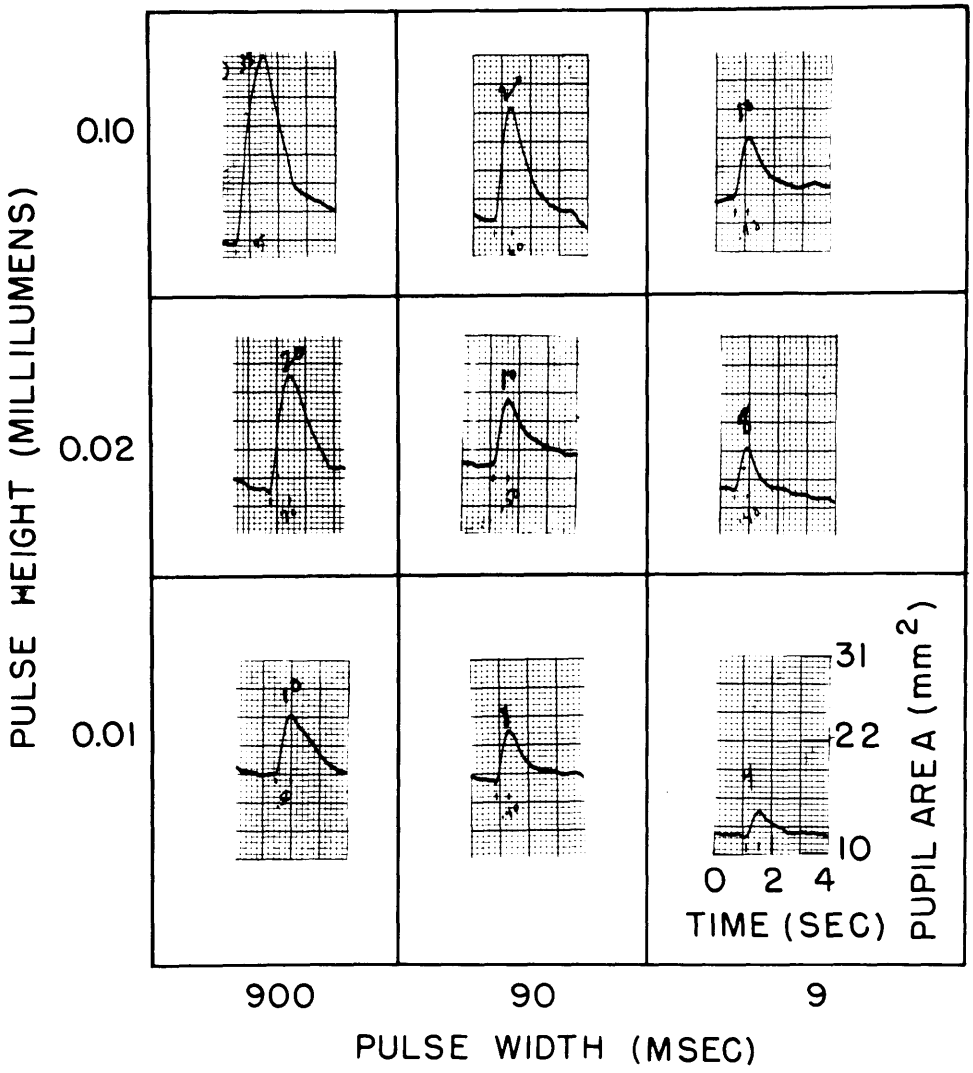

Fig. XIX-19. Organization of an experiment.

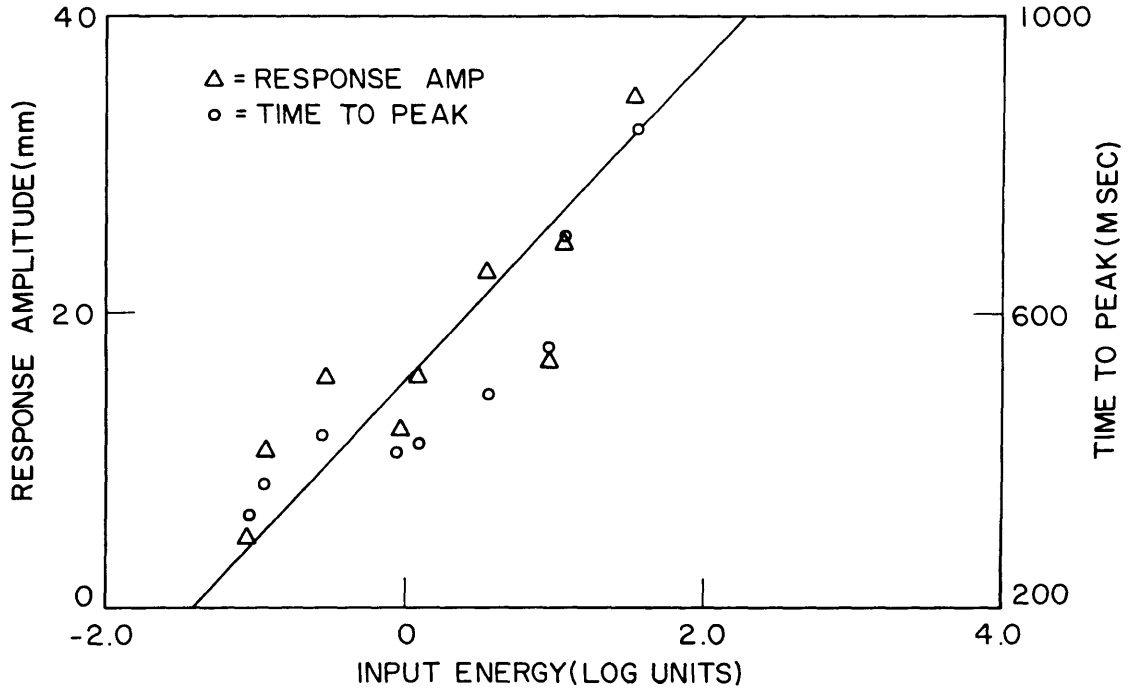

Fig. XIX-20. Averaged values of response amplitude and time to peak as a function of stimulus input energy.

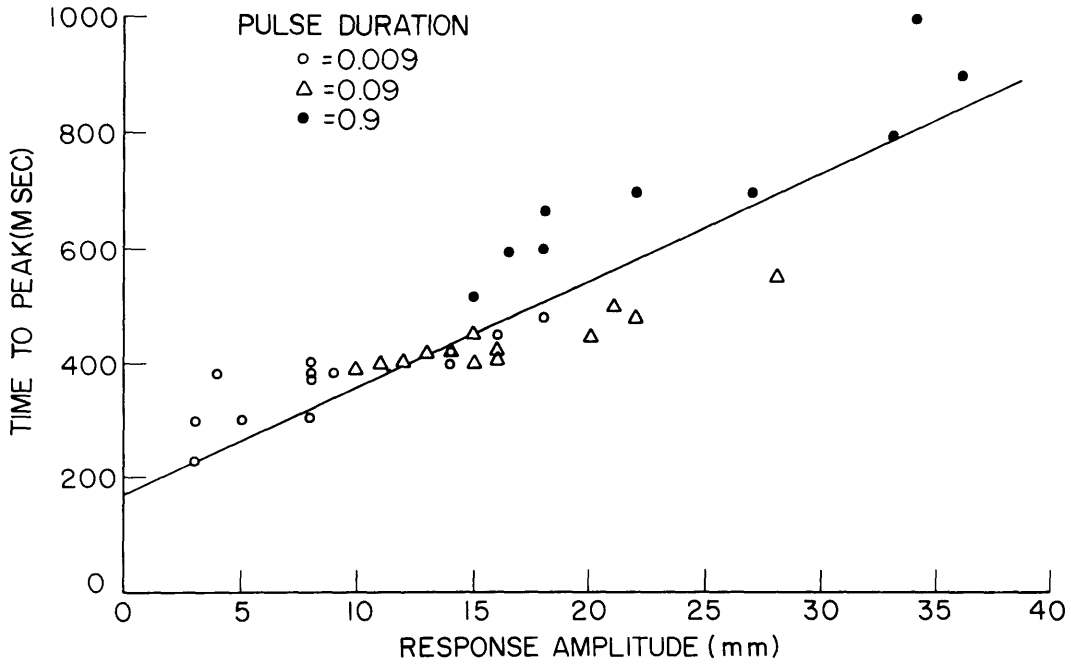

Fig. XIX-21. Time to peak of response plotted as a function of the response amplitude. Note points for differing pulse durations.

relationship between time to peak and response amplitude with both individual and averaged values, and the specific pulse duration is indicated. Since the pupil weighting function does not have a constant time to peak, the hypothesis put forward is disproved. Note, however, that the recent experiments were not made under strict dark adaptation, as were the original experiments. Fortunately, one of us (H.V.D.T.) is author of the hypothesis, and therefore no scientific controversy will ensue.

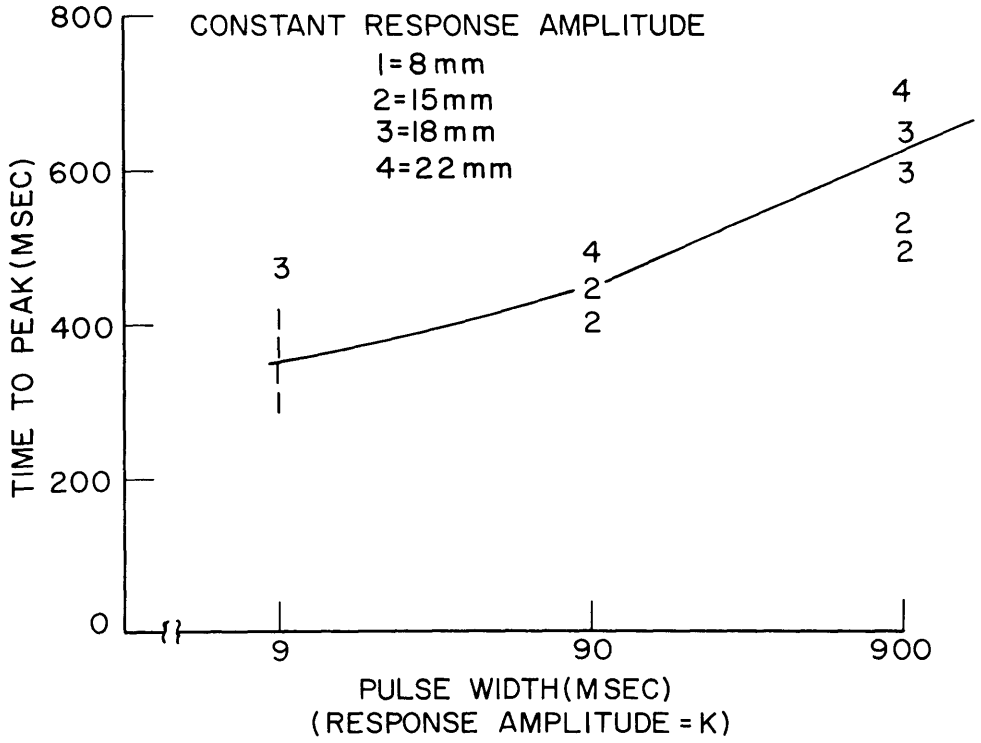

Fig. XIX-22. Time to peak as a function of pulse duration. Note the four different constant response amplitudes plotted.

It was thought to be of interest to see if equal response amplitudes that result from different combinations of stimulus duration and amplitude showed any significant dependency of time to peak on stimulus duration. The response of similar heights in the reversed diagonal were compared, and as Fig. XIX-22 demonstrates, if any dependency does exist, it is small until very wide pulses are used.

In other experiments, some of which are discussed in Section XIX-D, we are attempting to carefully define the areas of behavior of the pupil system wherein linear theory is helpful, and areas wherein various nonlinear approaches are more relevant.

The authors are grateful to Warren S. McCulloch for encouragement and support, especially in May 1960, when these experiments were initiated.

L. Stark, L. H. Van Der Tweel, Julia H. Redhead

(Dr. L. Henk Van Der Tweel has been a visitor from Laboratorium voor Medische Physica, Universiteit van Amsterdam, The Netherlands.)

References

1. L. H. Van Der Tweel and J. J. Denier Van Der Gon, The light reflex of the normal pupil of man, Acta Physiol. Pharmacol. Neerlandica 8, 69 (1959); see Fig. 15.

F. PUPIL SIMULATION

The goals of a servoanalytic description of the pupil system are a concise statement of experimental data and a deeper understanding of the physiological mechanisms associated with observed responses. Valuable by-products of model-making are the clarification of one's concepts and the suggestion of new experiments.

A digital-computer program, BIOSIM, provides a language to simulate a very general class of systems. Any model of the pupil system should include nonlinearities, such as saturation and the asymmetry of the system response to fast positive and negative light changes. Figure XIX-23 shows pupil step responses in either direction. Also shown

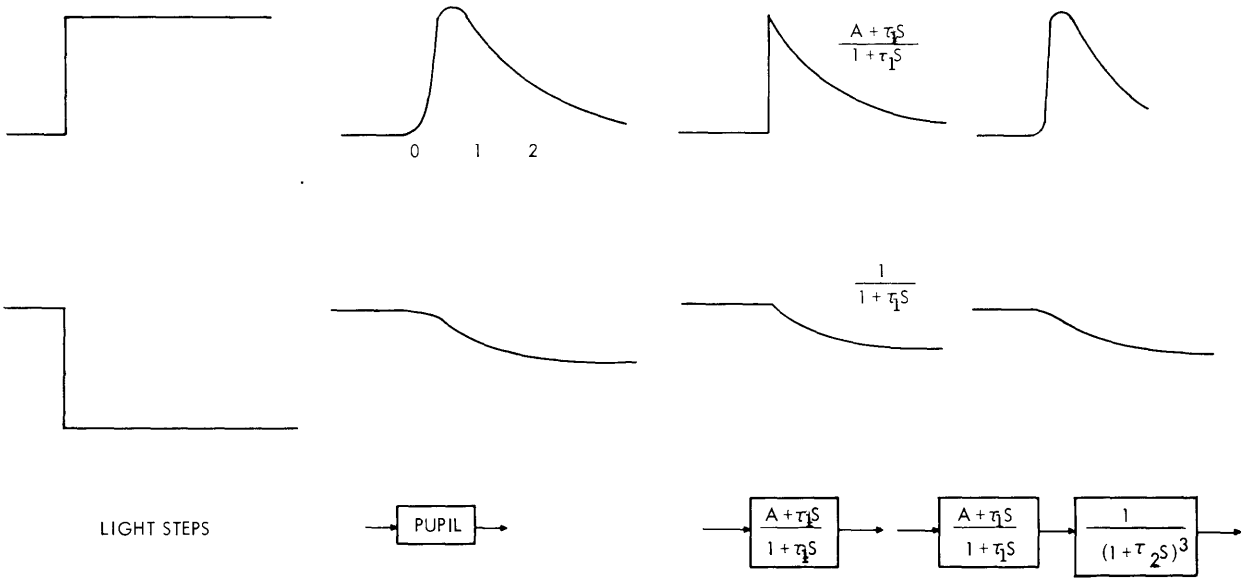

Fig. XIX-23. Experimental pupil responses to positive and negative light steps. Shown for comparison with pupil response are step responses of a triple lag, a lead lag, and a lead lag plus a triple lag.

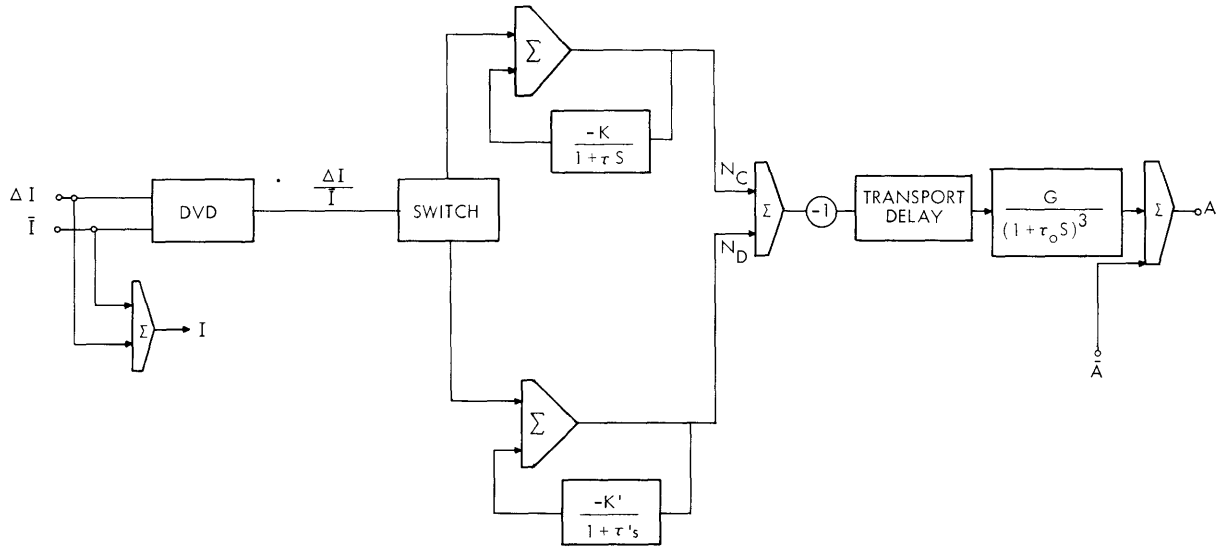

Fig. XIX-24. BIOSIM Mark I model of the pupil.

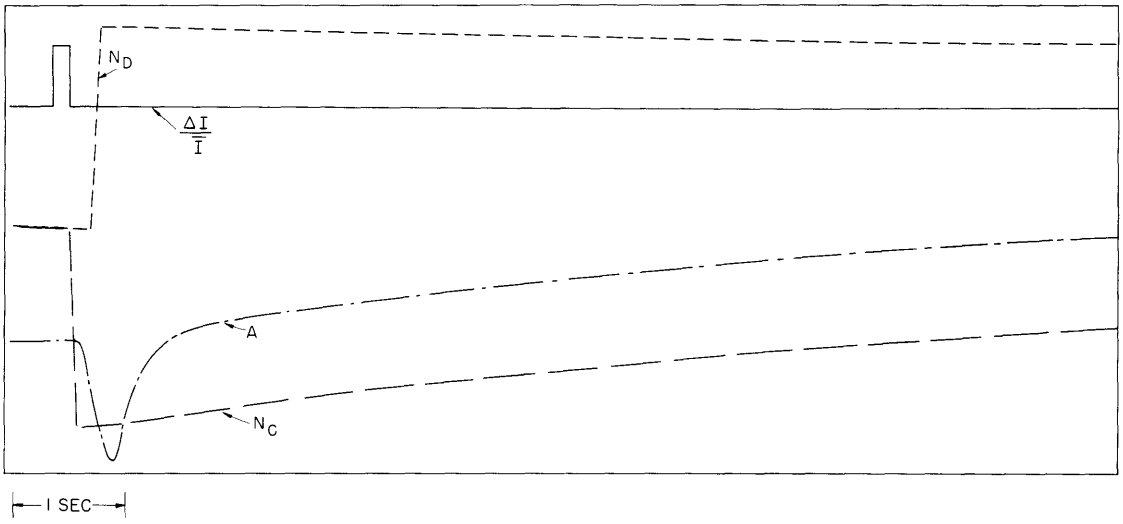

Fig. XIX-25. Responses of BIOSIM Mark I model to input steps. Since the model is piecewise linear, it superposes positive and negative step responses to form a pulse response.

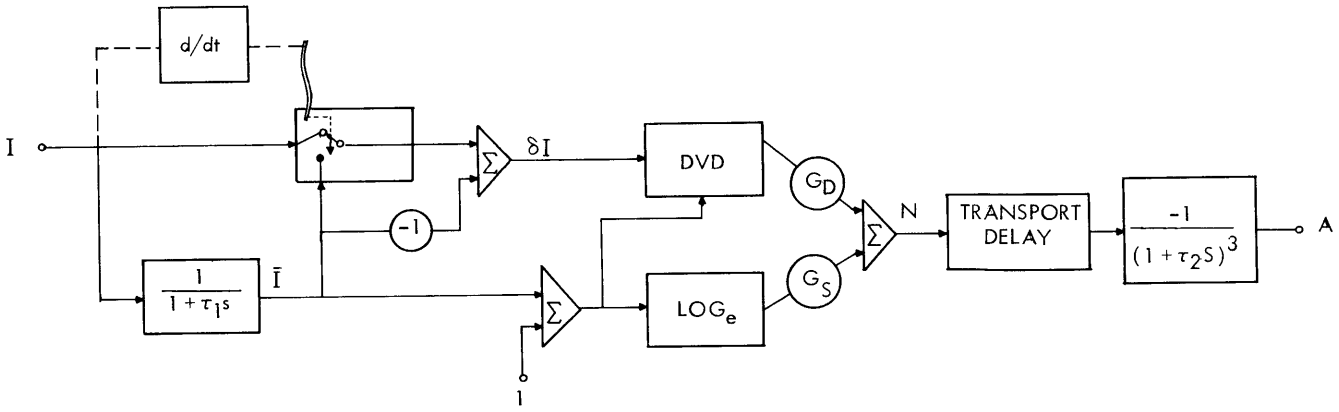

PARAMETERS

τ_1	$\approx$ 2 SEC
τ_2	$\approx$ 0.1 SEC
G_D	$\approx$ 2.5
G_S	$\approx$ 0.5
DELAY	$\approx$ 0.2 SEC

Fig. XIX-26. BIOSIM Mark II model of the pupil.

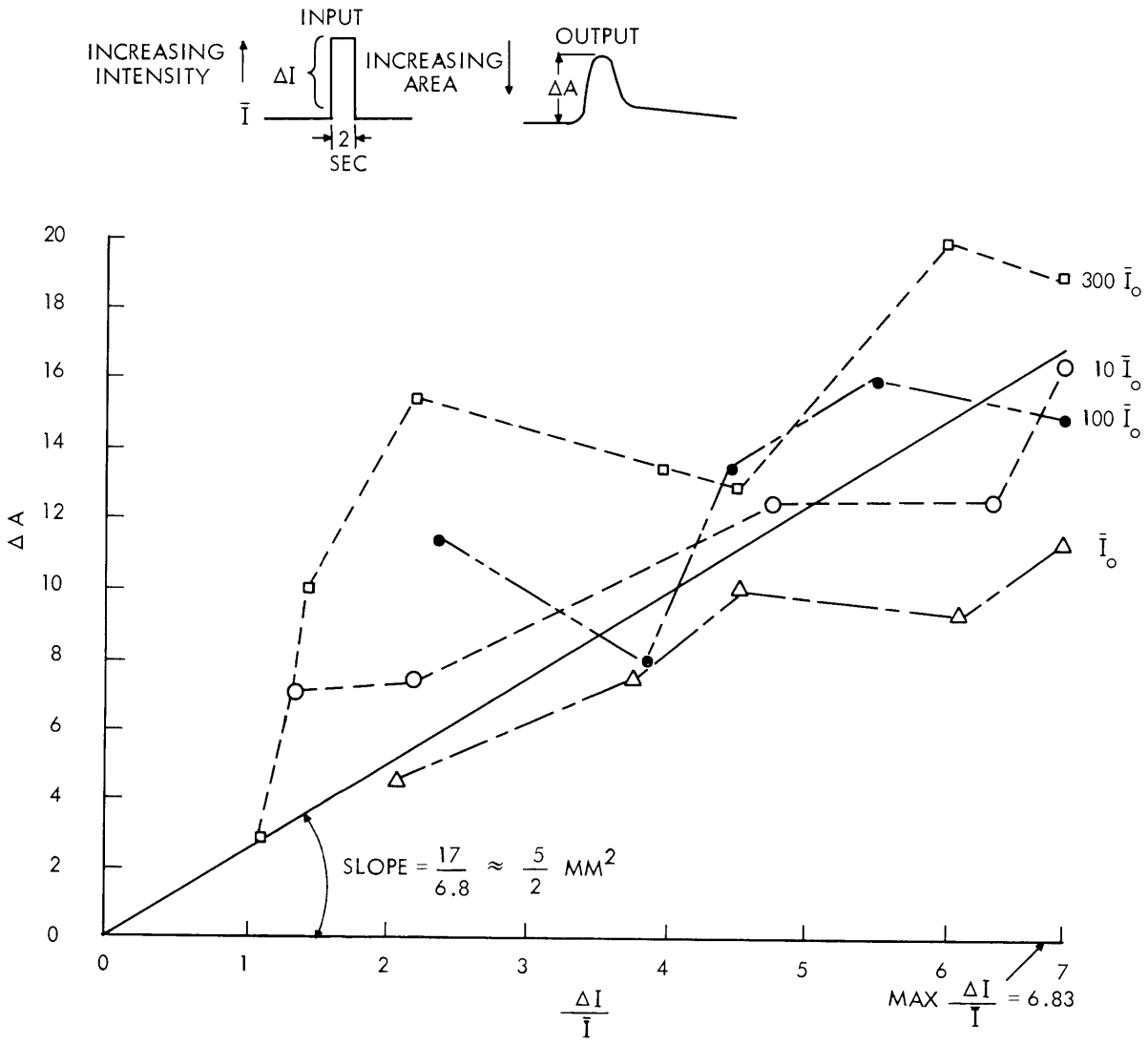

Fig. XIX-27. Experimental determination of G_D.

for comparison are two step responses of the lead-lag system function $(A+\tau_1 S)/(1+\tau_1 S)$, and the system function coupled with a triple lag, $(A+\tau_1 S)/(1+\tau_1 S)(1+\tau_2 S)^3$.

The BIOSIM Mark I model of the pupil is shown in Fig. XIX-24. It is piecewise linear in its response to ΔI, with a switch separating the positive and negative variations of ΔI and sending them through different linear systems. The resulting outputs are summed, delayed, passed through the third-order system function, and then summed with mean area ($\bar{A}$) to yield the output. The divide operator was originally included to account for scale compression, but it was not functional, since mean intensity ($\bar{I}$) was not varied in these first runs. Parameters for the transport delay and the triple lag were established from frequency-response data. The transfer functions in the parallel channels were chosen to simulate the characteristic shapes of the responses to steps as shown in Fig. XIX-23. We thought that only a simple change of parameter would account for asymmetry. We also thought that these transfer functions were related to light and dark adaptation, and time constants of 12 sec and 120 sec were assigned from experimental data of visual-adaptation experiments.

The step responses of the model are shown in Fig. XIX-25 and several important discrepancies at once are apparent. The time constants are tenfold too great, and thus the applicability of visual adaptation data to the pupil system is questioned. Because of the particular asymmetry in the pupil response, the dilatation behavior for short times

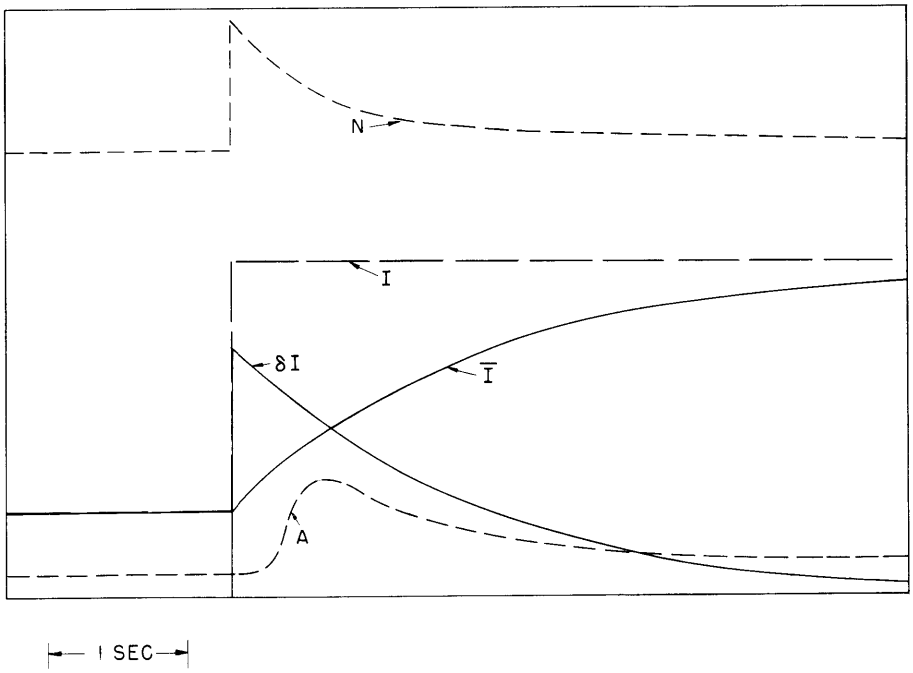

Fig. XIX-28. Response of BIOSIM Mark II model to light input step.

cannot be fitted by any arrangement of lead-lag parameters but needs a simple lag $1/(1+\tau S)$, with $\tau \approx 2$.

The BIOSIM Mark II model represents our direct attempt to simulate input-output experimental pupil data without consideration of actual internal physiological mechanisms. Figure XIX-26 shows how mean intensity is computed by a $1/(1+\tau_1 S)$ function that may be thought of as performing a weighted time average of the input. By subtracting $\bar{I}$ from the input, we obtain a signal, δI, that is a measure of fast deviations of input from mean level. A switch serves to make this $\delta I = 0$ whenever the derivative of intensity is negative. In that case only the mean-intensity level along the lower path is transformed to an area. When the switch is up, the δI signal is also transmitted and serves to give the characteristic pupil response to a positive light step.

The divide, $\frac{\delta I}{\bar{I}+1}$, and $\log[(\bar{I}+I)]$ operators serve as scale-compression functions that roughly approximate actual pupil saturations; the added constant, 1, keeps these functions well-behaved at the origin $\bar{I} = 0$.

An experiment performed to obtain the scale factor, or gain G_D, is shown in Fig. XIX-27, with a straight line fitted to quite variable data. In addition to experimental inaccuracies, the assumption as to the form of scale compression to be used may be erroneous.

The light step response of the BIOSIM Mark II model is shown in Fig. XIX-28 and appears to agree with the observed pupil response, except for a discrepancy in steady-state level. There is also a hidden difficulty in the switch in this model which will require further analysis and experiment to eliminate it.

I. Sobel, A. A. Sandberg, L. Stark